Graphical Abstract

Experimental assessment of a pilot-scale gasification plant fueled with olive pomace pellets for combined power, heat and biochar production

Roque Aguado, Antonio Escámez, Francisco Jurado, David Vera

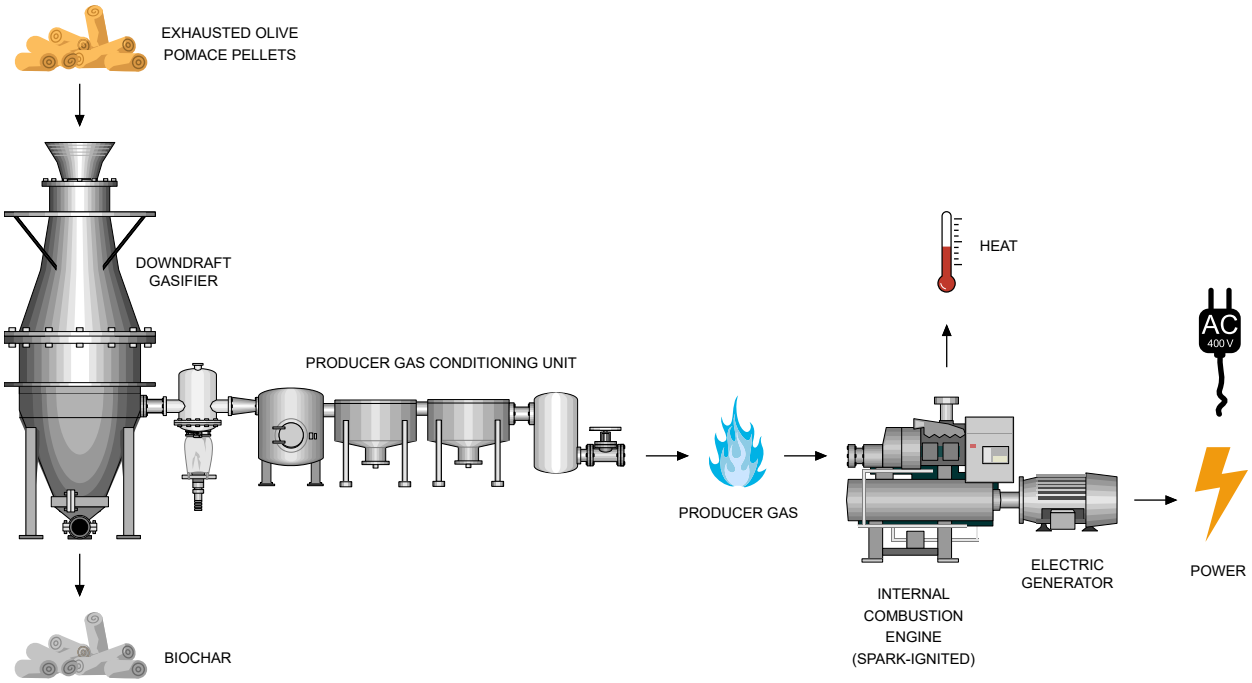

Highlights

Experimental assessment of a pilot-scale gasification plant fueled with olive pomace pellets for combined power, heat and biochar production

Roque Aguado, Antonio Escámez, Francisco Jurado, David Vera

- A gasification plant is tested for combined production of power, heat and biochar
- Exhausted olive pomace pellets are used as feedstock for a downdraft gasifier
- The technical feasibility of gasifying exhausted olive pomace pellets is demonstrated
- Dynamic plant performance data are provided under partial and full load operation
- The charcoal from the gasifier exhibits advantageous properties for agronomic use

Experimental assessment of a pilot-scale gasification plant fueled with olive pomace pellets for combined power, heat and biochar production

Roque Aguado, Antonio Escámez, Francisco Jurado, David Vera*

Departamento de Ingeniería Eléctrica, Escuela Politécnica Superior de Linares, Universidad de Jaén, Avda. de la Universidad s/n, 23700 Linares, Spain

Abstract

This research work examines the performance of an experimental gasification plant fueled with exhausted olive pomace pellets for the concurrent production of electricity, heat and biochar in the olive oil industry. The gasification plant consists of an air-blown downdraft fixed-bed gasifier that generates a lean fuel gas, termed producer gas, in a self-sustaining autothermal process. After conditioning of the producer gas in a cooling and cleaning unit, a four-stroke spark-ignition engine coupled to an electric generator is eventually used as power generation unit. An extensive experimental assessment of this facility was performed under partial and nominal load operation and was supplemented by a physicochemical analysis of the carbonaceous solid material discharged from the gasifier. The mass and energy balances of the gasification plant were calculated, including the carbon conversion efficiency and diverse energy conversion efficiencies. The results revealed an overall stable operation of the gasification plant in terms of composition and heating value of the producer gas and cogenerative production of electricity and heat in the engine–generator set. Under nominal operating conditions, the net electrical efficiency of the gasification plant was 12–13%, with an average carbon conversion efficiency of the biomass feedstock into producer gas just above 80% and an average cold gas efficiency close to 70%.

Keywords: Downdraft gasifier, Producer gas, Spark-ignition engine, Distributed generation, Bioenergy, Biochar

1. Introduction

Olive cultivation and olive oil extraction constitute a major cultural and economic activity in the Mediterranean basin, where about 95% of the world's olive oil production is concentrated [1].

*Corresponding author

Email addresses: ramolina@ujaen.es (Roque Aguado), aescamez@ujaen.es (Antonio Escámez), fjurado@ujaen.es (Francisco Jurado), dvera@ujaen.es (David Vera)

Olive groves occupy around 10 million hectares in the Mediterranean countries [2]. In particular, the largest area under olive groves worldwide is located in Spain, with over 2.5 million hectares [2], accounting for more than half of the total land area dedicated to this crop in Europe. In terms of olive oil production, Spain is also the world's leading country, with a yearly production of about 1.3 million tonnes on average in the last fifteen years (2007–2022), representing around 50% of the world's olive oil production [1]. The largest number of olive oil producers within Spain is located in Andalusia, with over 800 oil mills and roughly 75% of the national olive oil production [3]. However, it is worth noting that the Spanish olive oil production is heavily concentrated in Andalusia's hinterland, with the province of Jaén alone accounting for around 25% of the total olive grove area nationwide and responsible for about 35–40% of the national olive oil production [4]. In fact, the province of Jaén devotes nearly all of its agricultural land area for growing olive trees [5]. In no other part of the European continent can such a concentration and continuity of woody evergreen crops be found [5].

Nowadays, the vast majority (~90%) of olive oil mills in Spain operate through the two-phase continuous centrifugal oil extraction process [6], which represents the predominant extraction process with more than 95% of the domestic olive oil production [7]. In the two-phase olive oil extraction process, a by-product known as wet olive pomace is produced at massive rates [6]. It is estimated that roughly 70–75% by weight of the processed olives become pomace, a thick sludge with a remarkably high moisture content (60–70%, wet basis) made up of olive pulp, skin, crushed pits and some remaining olive oil [8–10]. The rest of the olive oil contained in the wet pomace, known as crude olive pomace oil, needs to be extracted with the help of industrial organic solvents, usually hexane. To this end, the wet pomace is continuously evacuated from oil mills and transported to olive pomace oil extraction plants in tanker trucks. The wet pomace is then unloaded into large ponds located in the vicinity of these plants, where it is stored and initially air-dried to a certain extent. However, an additional energy-intensive drying stage in large-scale continuous rotary drum dryers is typically required before eventual extraction of the crude olive pomace oil with

the organic solvent, leaving exhausted olive pomace as by-product. The average production of exhausted olive pomace in Andalusia ranges between 1.2–1.5 million tonnes per year [11]. Thus, a wide availability of this by-product from the extraction process of crude olive pomace oil is guaranteed at relatively low cost (10–25 €/t) [12]. The exhausted olive pomace can be used as fuel to the meet the energy demands of the olive oil industry. Nevertheless, long-distance transportation of such biomass feedstock is often limited due to economic penalties, and thus, the demand should be met by local supply. This constraint encourages a greater number of small-scale decentralized bioenergy plants, rather than fewer large-scale conventional biomass-fired power plants.

As a result of the growing environmental awareness concerning waste management and recovery in the olive oil industry, biomass gasification has recently attracted increasing attention to foster the circular economy concept by closing the loop of olive oil production through combined heat and power (CHP) generation (also known as cogeneration) in a decentralized manner [13–18]. Gasification is a thermochemical conversion process, whereby a carbonaceous solid feedstock is partially oxidized by a gasifying agent and converted into a gaseous fuel. The gaseous product of gasification with pure oxygen, carbon dioxide and/or steam as gasifying agent is generally referred to as synthesis gas or syngas, a mixture of combustible gases with minor amounts of non-combustible gases, such as carbon dioxide and water vapor [19]. However, if ambient air is used as gasifying agent, a substantial amount of nitrogen is present in the gas mixture as well, which leads to a highly diluted synthesis gas, the term used for which is producer gas [19]. In the particular case of air-blown gasification, the producer gas is mainly composed of carbon monoxide (CO), hydrogen (H_2), carbon dioxide (CO_2), methane (CH_4), nitrogen (N_2), water vapor (H_2O) and smaller fractions of other light hydrocarbons that are in gaseous state at 20 °C (mostly, C_2 to C_4), hereinafter designated collectively as C_nH_m. These light hydrocarbons mainly include C_2H_2 and, to a lesser extent, C_2H_4 [20, 21]. Other minor compounds that may also be present at trace levels include, but are not limited to: ammonia (NH_3), hydrogen cyanide (HCN), hydrogen sulfide (H_2S), carbonyl sulfide (COS) and a variety of cyclic and aromatic hydrocarbons, generically

referred to as tars [22, 23].

For distributed power generation in biomass gasification plants, ambient air is usually preferred over pure oxygen or steam as gasifying agent. Even though gasification with pure oxygen avoids nitrogen dilution, thereby leading to a synthesis gas with a superior energy density to that of producer gas [24], an air separation unit is typically not considered for small-scale CHP plants, because of the excessively high capital and operational costs offsetting any advantage [14]. In air-blown gasification, the feedstock supplied to the gasifier is partially oxidized in an autothermal process. The exothermic oxidation reactions provide enough heat to sustain the endothermic reduction reactions required for the producer gas formation [24, 25]. The producer gas from gasification, once conditioned, can be used as fuel for decentralized electricity and/or heat production through internal combustion engines, gas turbines or even fuel cells [21]. However, internal combustion engines are nowadays the most usual option for small-scale biomass gasification CHP plants, due to their numerous advantages as compared to other power generation units, such as low capital cost, modularity, reliability, good part-load performance and high operating efficiency [19].

Among the existing designs for gasification reactors, downdraft gasifiers are arguably the preferred choice for distributed generation in small-scale CHP plants (< 1 MW_{th}) [24, 26–28], due to their relatively simple construction, low investment cost, reliable operation and applicability to numerous biomass feedstocks [24, 29, 30]. In downdraft gasifiers, the moving bed of solid feedstock is directed together with air in the downward direction, undergoing several thermochemical reactions while passing through four different zones, namely drying, pyrolysis, oxidation and reduction. The producer gas from biomass gasification in air-blown downdraft reactors is characterized by a relatively low energy density (LHV = 4–6 MJ/Nm^3) as a result of the nitrogen dilution effect [24, 26]. However, a great advantage of downdraft gasifiers over most other designs is their lower tar production rate, with an average value of only around one gram of tar per normal cubic meter of producer gas [24, 31], since the tars formed in the pyrolysis zone are burned immediately

after in the oxidation zone in a phenomenon called flaming pyrolysis [24]. Although tar gases are combustible, they can intensely foul and eventually block the pipelines and mechanical equipment downstream of the gasifier by condensing into a thick, sticky, highly viscous liquid [23, 32, 33]. Hence, a conditioning unit is usually included to reduce the content of tar and other impurities in the producer gas to acceptable levels [26, 34, 35]. As a result of their comparatively lower tar production, gasification plants for decentralized power generation using downdraft gasifiers require a simpler and less robust producer gas conditioning unit with lower energy consumption [24, 31].

Apart from electricity and heat, another potentially valuable output of biomass gasification is a recalcitrant carbonaceous solid by-product known as biochar. As a result of its outstanding physicochemical properties, this by-product could be used as soil amendment in the olive grove [36–39], providing a wide range of benefits:

1. Due to its high specific surface area and pore volume [36, 40], biochar improves the water holding capacity of the agricultural soil and retention of dissolved nutrients [39, 41]. This property can be advantageous for olive groves to resist droughts and reduce water wastage [42].
2. The use of biochar as soil amendment prevents erosion and leaching [41]. Biochar can also absorb poisonous substances, producing a depurative action to the soil [42].
3. Biochar supports plant growth and can increase crop yield up to 10% on average [39]. If deposited on the agricultural soil, biochar boosts the rhizosphere by promoting the development of a large and diversified microbial community, including the microorganisms that support plant growth [36, 39, 43, 44].
4. From an environmental perspective, biochar use as soil amendment constitutes a carbon sink, namely, a long-term carbon sequestration in the olive grove [36, 38, 40, 41, 45, 46]. In other words, a substantial part of the carbon content that had earlier been captured and retained by olive trees is eventually returned to the soil, avoiding its short-term emission back into the atmosphere in the form of carbon dioxide and contributing to reducing global

warming [36, 42].

Despite all these advantages, it is worth noting that biochar from gasification may have significant amounts of environmentally hazardous substances. Biomass gasification at temperatures below 700 °C is conducive to higher yields of contaminants from pyrolysis reactions, generically designated as tars, which include polycyclic aromatic hydrocarbons (PAHs), polychlorinated biphenyls (PCBs), dioxins and furans [45, 47]. As these contaminants have toxic effects that may pose a risk to soil faunal communities [45], the chemical safety of biochar must be certified before use as soil amendment [39]. The most widely used biochar certification standards are the International Biochar Initiative (IBI) and the European Biochar Certificate (EBC) [47–49].

A number of experimental works have been devoted to evaluating the performance of pre-commercial downdraft gasifiers with a variety of biomass feedstocks, including wood chips, chunks or pellets from diverse tree species [20, 35, 50–70], sunflower seeds [61], switchgrass [62], rice husks [63, 71–75], sugarcane bagasse [31, 34], coconut shells [30, 31, 34, 76], hazelnut shells [77], walnut shells [78], olive pits and tree pruning [13, 16–18], corncobs [21, 30, 70, 72, 79] or cotton residues [25, 42, 72]. However, very little work has been done on gasification of olive pomace [80, 81], despite the high availability of this by-product from olive oil production in the countries surrounding the Mediterranean basin. Indeed, it is not known of previous experimental research work on pilot-scale CHP plants based on downdraft gasifiers fueled with olive pomace pellets. Moreover, it should be noted that the majority of the research articles cited above mostly focus on the biomass gasifier, and very few works in the scientific literature are available on small-scale biomass gasification CHP plants including detailed mass and energy balances, discussion of conversion efficiencies and losses, dynamic plant operation data as well as experimental results on biochar production and characterization. Accordingly, the aim of this work is to conduct a comprehensive experimental performance evaluation of a pilot-scale gasification plant for combined heat, power and biochar production in the olive oil industry using exhausted olive pomace as feedstock, given the large supply of this by-product of olive oil production. It is noteworthy that the

results from this work are not limited to a single region or country and can therefore be applied to any olive oil producing region worldwide. In addition, unlike most of the aforementioned experimental works, which are mainly focused on the behavior of the gasifier, a holistic approach has been adopted to evaluate the performance of the gasification plant as a whole. The instantaneous dynamic behavior of the gasification plant during operation is investigated through real-time measurements of all the involved performance parameters. In this context, the instant interaction between the downdraft gasifier and the engine–generator set is considered. While this work focuses on the cogenerative production of electricity and heat from exhausted olive pomace pellets, an additional investigation was conducted for quantification and physicochemical characterization of the charcoal discharged from the gasifier.

2. Methodology

The methodological approach for this work is divided into several parts. First, the biomass used as feedstock for the gasification process is physicochemically characterized. The pilot-scale gasification plant, in addition to the instrumentation, automation and data logging equipment are described thereafter. Finally, the operating procedure and governing equations for plant performance evaluation and uncertainty assessment are presented.

2.1. Biomass feedstock

The performance of the gasification process is heavily influenced by the physicochemical properties of the biomass feedstock. Fixed-bed gasifiers are more suitable for raw materials with particles sizes ranging between 3–51 mm [24]. A majority of particles should ideally have sizes between 10 mm and 25 mm [50, 56]. Oversized particles should not exceed 5 mm, and fines (under 10 mm) are typically limited to a maximum of 10% by weight of the feedstock [50]. This is because fine particles in downdraft gasifiers are conducive to the formation of ash clinkers, which disturb the optimal flow in the gasifier bed, leading to excessive pressure drops, low temperatures

in the reduction zone and unstable operation [79, 82]. In this regard, pelletization is a suitable option for biomass conditioning and densification prior to being supplied to downdraft gasifiers, allowing the production of stable dry fuels of uniform size with higher energy density [61]. This work proposes using exhausted olive pomace as feedstock for the gasification plant. However, as about 80% by weight of crude exhausted olive pomace have particle sizes smaller than 3 mm, the feedstock must be pelletized in advance.

The exhausted olive pomace pellets used as feedstock for the gasification plant were supplied by a local biomass trading company in the municipality of Linares, Andalusia, Spain. As can be seen in Fig. 1, the pellets are cylindrical in shape, with diameters of about 10 mm and lengths ranging from 10 mm to 35 mm. Table 1 presents several physicochemical properties of the exhausted olive pomace pellets that are of interest for the gasification process. As a result of the heterogeneous nature of this feedstock, property ranges with minimum, average and maximum values were determined from a wide variety of samples. The proximate analysis includes the moisture content, ash content, volatile matter and fixed carbon; while the ultimate analysis, determined according to standard ISO 16948:2015, indicates the carbon, hydrogen, nitrogen, sulfur, chlorine and oxygen contents of the feedstock. A Parr automatic isoperibol calorimeter (series 6400, Moline, IL, USA) was used to experimentally determine the higher heating value of the feedstock in accordance with standard ISO 18125:2017. However, in thermochemical conversion processes it is more reasonable to use the lower heating value (LHV) of the feedstock, as it excludes the heat of vaporization of water, which does not contribute to the actual heating value of the fuel [16]. The lower heating values reported in Table 1 were estimated from the experimentally determined higher heating values and the proximate and ultimate analyses. Another important physical property of exhausted olive pomace pellets is the bulk density (ρ_f^*), which is defined as the mass of feedstock packed loosely in a container divided by the total volume occupied. This property was rigorously measured based on standard ISO 17828:2015. A high bulk density of the biomass feedstock is desirable, as it involves a high energy content per unit volume [78].

Figure 1: Exhausted olive pomace pellets used as feedstock for the gasification plant.

Table 1: Physicochemical properties of exhausted olive pomace pellets.

Proximate analysis, wt. %	Min.	Avg.	Max.
Moisture, as received	4.80	9.88	13.80
Ash, dry basis	5.40	7.20	9.20
Volatile matter, dry basis	70.24	73.53	76.67
Fixed carbon, dry basis	16.43	19.27	22.36
Ultimate analysis, wt. % dry basis	**Min.**	**Avg.**	**Max.**
Carbon	47.49	51.02	55.44
Hydrogen	5.26	5.88	6.50
Nitrogen	0.40	0.95	2.20
Sulfur	0.07	0.14	0.24
Chlorine	0.12	0.26	0.40
Oxygen (by difference)	31.04	34.55	38.86
Higher Heating Value (HHV), MJ/kg	**Min.**	**Avg.**	**Max.**
As received	17.64	18.81	19.98
Dry basis	19.12	20.07	20.94
Lower Heating Value (LHV), MJ/kg	**Min.**	**Avg.**	**Max.**
As received	16.06	17.23	18.44
Dry basis	17.68	18.61	19.55
Bulk density (ρ_f^*), kg/m^3	**Min.**	**Avg.**	**Max.**
As received	681.3	698.7	716.1

2.2. *Plant description*

For the purpose of this research work, a small-scale biomass gasification plant manufactured by Ankur Scientific Energy Technologies Pvt. Ltd. (India) was installed in the proximity of an experimental olive oil mill (IFAPA Centro "Venta del Llano", Andalusia, Spain). The gasification plant consists of a downdraft fixed-bed gasifier, a producer gas cooling and cleaning unit and a four-stroke spark-ignition engine coupled to an electric generator as power generation unit. The downdraft gasifier is a throatless stratified reactor (also called "open-top" or "topless") that operates at ambient pressure. The downdraft gasifier under autothermal operation converts the carbonaceous feedstock into producer gas, a lean fuel gas that, after a mild conditioning stage, is used to drive a conventional engine–generator set manufactured by Weifang Naipute Gas Genset Co. Ltd. (China). The prime mover is a naturally aspirated, inline four-cylinder spark-ignition engine with a modified carburetor in order to run on the producer gas from gasification. The engine cylinders were designed to operate with a fixed compression ratio of 9.6:1. The engine drive shaft is directly connected to an alternating current (AC) generator. The electric power generator is a brushless self-excited three-phase synchronous generator equipped with an automatic voltage regulator (AVR). In order to generate electric AC power with a constant frequency of 50 Hz, the rotational speed of the engine is maintained at 1500 rpm using a speed governor. The technical specifications of the engine–generator set fueled with producer gas from the downdraft gasifier are reported in Table 2.

Table 2: Main features and nominal operating parameters of the engine–generator set.

Internal combustion engine		**Electric generator**	
Type	Four strokes, spark-ignited	Type	Synchronous, brushless
Cylinder number	Four	Pole number	Four
Arrangement	Inline	Excitation mode	Shunt (self-excited) / AVR
Rated power	15 kW	Rated active power	10 kW
Bore × stroke	90 × 100 mm	Rated current	18 A
Total displacement	2.54 L	Rated voltage	400 V
Rated speed	1500 rpm	Rated frequency	50 Hz
Compression ratio	9.6:1	Rated power factor	0.8 lagging

A 3D layout of the biomass gasification plant is displayed in Fig. 2. The downdraft gasifier (4) is made of stainless steel with an internal refractory lining and is coupled to a duct for discharging the gaseous product, while the solid by-product is removed from the bottom. The hot producer gas leaving the gasifier typically contains traces of fly ash, soot, tar, moisture and other impurities that, if not removed, can lead to severe fouling and corrosion issues to all mechanical equipment. Therefore, the gaseous fuel must be cooled down to near ambient temperature and cleaned up to meet the requirements reported by the manufacturer of the internal combustion engine [18], which are outlined in Table 3. An advantage of using internal combustion engines as power generation unit over gas turbines or fuel cells is a greater tolerance to contaminants [83, 84]. In fact, engines can run on producer gas with tar contents up to about 50–100 mg/Nm^3 [23, 26, 68, 84, 85] and contents of suspended particulate matter below 50 mg/Nm^3 [26, 68, 85]. In order to meet such cleaning requirements, the gasification plant incorporates a producer gas conditioning unit downstream of the gasifier with the following components. First, a wet scrubber (5) drastically reduces the producer gas temperature by spraying a pressurized water jet with a nominal flow rate of 150 l/min. The fine water droplets sprayed by the wet scrubber nozzle remove soot and fly ash particles together with the tars formed in the gasification process and, if present, ammonia and alkaline compounds, which dissolve readily in water. The producer gas then leaves the scrubber with a temperature of around 40–45 °C depending on the inlet gas and cooling water temperatures [16]. Rapid cooling in the scrubber also causes oversaturation of vapors and formation of a dense mist composed of small droplets of liquid water and tar particles. To eliminate this undesired mist and the remaining contaminants formed when vapors are cooled below their dew point, a coarse filter (6) filled with dry char, two fine filters (7) filled with sawdust and a safety filter (8) with a fabric bag are included, thus ensuring that the producer gas eventually meets the minimum conditioning requirements to power the engine–generator set (11). In addition, the gasification plant is equipped with a flare stack (9), which is an elevated vertical pipe for carrying the producer gas so that it can be safely discharged and burned off at a considerable height. A centrifugal blower is

used to provide the necessary suction to draw air through the gasifier, while the flow rate of air is manually controlled by means of a butterfly valve. The centrifugal blower is not shown in Fig. 2, but it is placed between units (8) and (9). During the producer gas conditioning process, water is contaminated with both dust and hundreds of different organic compounds [55, 86]. For that reason, the gasification plant also includes a waste water treatment unit to recover the contaminated water from the wet scrubber. The waste water treatment unit consists of several sand and charcoal filters (not included in Fig. 2), a cooling tower (1) and an open top water tank (2).

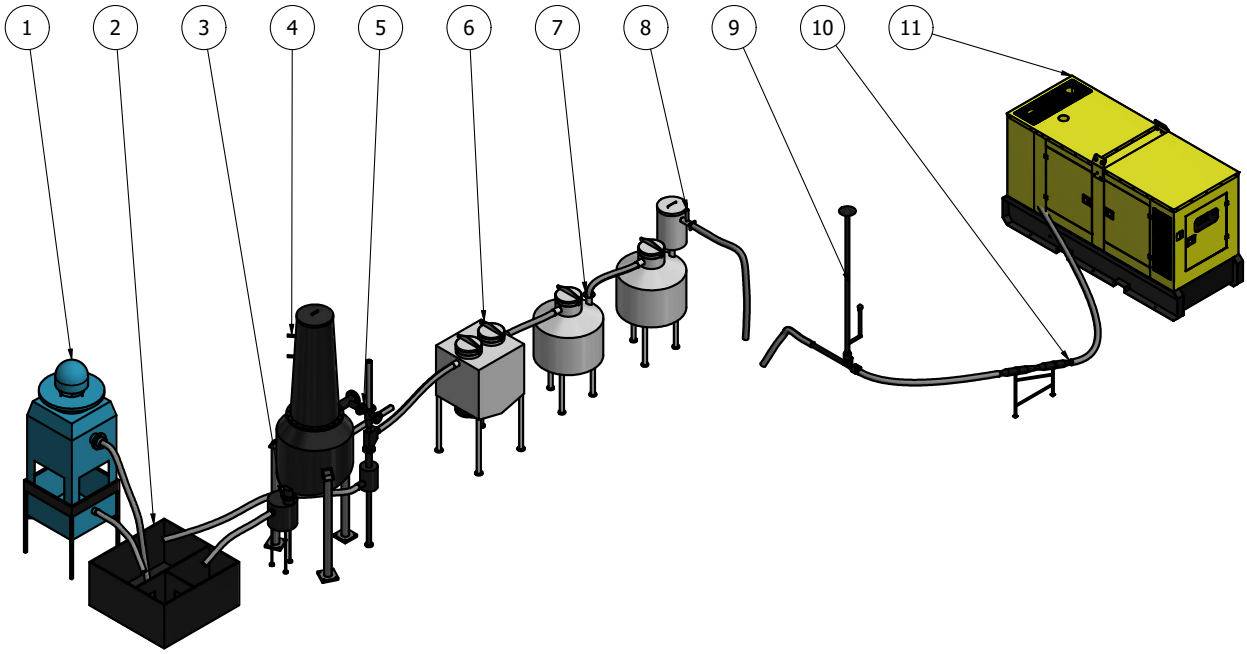

Figure 2: 3D layout of the biomass gasification plant: ① cooling tower; ② water tank; ③ char removal unit; ④ downdraft fixed-bed gasifier; ⑤ wet scrubber; ⑥ coarse filter; ⑦ fine filters; ⑧ safety bag filter; ⑨ flare stack; ⑩ Venturi flow meter; ⑪ spark-ignition engine–generator set.

Table 3: Minimum conditioning requirements of the producer gas for use as fuel in internal combustion engines.

Parameter	**Limit value**
Producer gas temperature	≤ 45 °C
Producer gas LHV	≥ 4.2 MJ/kg
Tar content	≤ 100 mg/Nm^3 (preferably ≤ 20 mg/Nm^3)
Particulate matter	≤ 50 mg/Nm^3
Hydrogen sulfide	≤ 20 mg/Nm^3
Water vapor	$\leq 5\%$ vol.

The balance of plant (BOP) includes electric motors of the hopper vibration mechanism, char scraper, char removal pump, scrubber pump, cooling pump, cooling tower fan and gas blower. Other components with significant electrical consumption are instrumentation and control and power electronics. The synchronous generator can be directly connected to the grid or to a load bank after reaching the nominal speed and, except for the circuit breakers, no other power equipment is necessary.

2.3. Instrumentation

In order to control and monitor all the relevant operational data, a series of thermocouples, pressure sensors, a portable syngas analyzer (Gasboard 3100P, Hubei Cubic-Ruiyi Instrument Co. Ltd., China) and a gas volumetric flowmeter were used.

The time-averaged mass flow rate of exhausted olive pomace pellets (i.e., feedstock consumption) was calculated according to Eq. (1), which considers constant pre-weighed batches of 6 kg that are loaded at intervals such that the volume decrease of feedstock inside the gasifier is fully replenished [18, 25, 30, 59].

$$\dot{m}_f = \frac{m_f}{\Delta t} \tag{1}$$

where m is the mass of the feedstock and Δt is the time interval at which pre-weighed batches are loaded. In other works [50, 78], the feedstock consumption is also estimated as a function of the volume decrease inside the gasifier, but using an indirect calculation method through the average bulk density of the feedstock.

A few calibrated K-Type (chromel-alumel) thermocouples were placed in several locations of the gasification plant: two internal cross-sections along the axis of the downdraft gasifier (pyrolysis and oxidation zones), at the reactor outlet and after the wet scrubber. The thermocouples were connected to the control panel in order to display the temperatures inside the gasifier in real time. Furthermore, a set of differential pressure sensors was installed to determine the pressure drops

across the gasifier bed and after each of the filters.

The volumetric flow rate of cold producer gas was measured by means of a calibrated Venturi flowmeter placed downstream of the producer gas conditioning unit [70]. The producer gas from gasification flowing through the Venturi meter can be safely treated as an incompressible flow, as the Mach number, defined by the ratio of the speed of the flow to the speed of sound, is much smaller than 0.3, and thus, compressibility effects become negligible, with errors below 1% [87]. A differential pressure sensor attached to the converging conical and throat sections of the Venturi flow meter records the pressure drop, which as evidenced in Eq. (2), becomes an indication of the volumetric flow rate of producer gas through the pipeline.

$$\dot{V}_{cg} = \frac{\pi}{4} d_1^2 \sqrt{\frac{2}{\rho_{cg}} \cdot \frac{p_1 - p_2}{\left(\frac{d_1}{d_2}\right)^4 - 1}} \tag{2}$$

where subscripts 1 and 2 refer to the converging conical and throat sections of the Venturi flow meter, respectively. The following empirical equation was reported by the manufacturer for calibration:

$$\dot{V}_{cg} = 23.144 \sqrt{\Delta p} \tag{3}$$

where $\dot{V}_{cg}$ is the volumetric flow rate of producer gas in m^3/h and Δp is the pressure drop across the throat in millimeters of water column (mmH_2O). The volumetric flow rate of air can be estimated by mass balance in accordance with Eq. (4), on the assumption that nitrogen in the input air is inert and the nitrogen content from the ultimate analysis of the feedstock can be disregarded [25, 38, 42, 64, 72, 78, 79, 88].

$$\dot{V}_{air} = \frac{T_{air}}{T_{cg}} \cdot \frac{p_{cg}}{p_{air}} \cdot \frac{y_{N_2,cg}}{y_{N_2,air}} \dot{V}_{cg} \tag{4}$$

where $\dot{V}_{air}$ and $\dot{V}_{cg}$ are the volumetric flow rates of intake air and cold producer gas, T_{air} and T_{cg}

are the absolute temperatures of air and producer gas, p_{air} and p_{cg} are the absolute pressures of air and producer gas, $y_{N_2,air}$ and $y_{N_2,cg}$ are the mole fractions of nitrogen in air and producer gas, respectively. Therefore, under identical conditions of temperature and pressure, the volumetric flow rate of nitrogen in the inlet air to the gasifier is assumed equal to the volumetric flow rate of nitrogen in the cold producer gas.

The gasification plant is provided with an in-line gas sampling point placed after the producer gas conditioning unit, next to the blower, where the portable syngas analyzer is connected. This instrument was used for simultaneous measurement of the volume concentrations of carbon monoxide (CO), hydrogen (H_2), carbon dioxide (CO_2), oxygen (O_2), methane (CH_4) and other light hydrocarbons (C_nH_m) in the sample gas, while the nitrogen (N_2) balance is calculated automatically by difference [21, 89]. Measurements of the volumetric composition of the producer gas are performed continuously at a user-specified time step and only require a flow rate of 0.06 m^3/h. The H_2 concentration is determined using a thermal conductivity detector (TCD) with a precision $\leq$ 3% full scale (FS). The CO, CO_2, CH_4 and C_nH_m concentrations are provided by a nondispersive infrared (NDIR) sensor with a precision $\leq$ 2% FS. The O_2 concentration is determined using an electron capture detector (ECD) with a precision $\leq$ 3% FS. Even though the producer gas also contains water vapor, there is no provision for measuring its concentration [33]. Thus, the volumetric composition of the producer gas is given on a dry basis.

The electrical performance parameters of the gasification plant were monitored using contactless power analyzers (Carlo Gavazzi CPA-050, Italy), which are capable of measuring a wide range of parameters, including active and reactive power, frequency, voltage, current, power factor ($\cos\varphi$) and total harmonic distortion (THD). These devices were used to measure the load profiles of the generator phases when connected to a resistive load bank [59], in addition to the electricity consumed by the ancillary equipment, also known as parasitic load consumption. As a three-phase unbalanced load is used at times, a different power analyzer must be used to monitor each phase.

2.4. Automation and data logging

The gasification plant is partially automated by means of a programmable logic controller (PLC). The control panel is designed to operate the following motors and drives: scrubber pump, char removal pump, hopper vibrator motor, blower motor, scraper motor, cooling pump and cooling fan.

Data logging and monitoring is driven by a re-programmable open-source software code that can be easily customized. In order to communicate with all the sensors of the gasifier and producer gas conditioning unit, ESP32 microcontrollers were used to send data via WiFi MQTT to a local server. The performance parameters of the electric generator were monitored using contactless power analyzers controlled by a STM32 microcontroller, which sends data via Modbus RTU. All the sensor data are received by the server and processed using Node-RED. InfluxDB database was used to store all the sensor data, because it is optimized for time series data. Finally, Grafana was used for data monitoring and visualization in customized dashboards. The data logging system was configured to record all the plant performance parameters at a preset interval of one second.

2.5. Operating procedure

The experimental procedure for operation of the gasification plant begins with the preparation of the biomass feedstock to the downdraft gasifier. The gasification plant operates in semi-batch mode, namely, the solid feedstock is intermittently loaded into the downdraft gasifier through the hopper in a batch operation [30, 50, 51, 78], while the producer gas flows continuously downstream. Initially, the gasification plant is thoroughly checked to ensure that all the filters, ducts and junctions are well sealed against air leakages, since the producer gas conditioning unit operates slightly below ambient pressure (between 85 and 95 kPa) [50, 78]. Then, a portable blowtorch is used to provide the gasifier with the required external heat input by igniting the feedstock across the entire cross section. Hereinafter, as the temperature rises, the gasification process becomes autothermal. In other words, the partial combustion of the feedstock supplied to the gasifier is able

to produce enough heat to sustain the high temperature atmosphere needed for the endothermic reactions that give rise to the formation of the producer gas to take place. While the feedstock moves downward due to gravity, airflow is induced through the reactor by a blower. A hopper vibration mechanism is driven by an electric motor at regular time intervals with the aim of maintaining a continuous downward movement of the feedstock inside the gasifier, thereby avoiding channeling and bridging through the gasifier bed [70]. Likewise, a scraper driven by an electric motor is installed in the lower part of the gasifier in order to facilitate char and ash discharge below the grate that supports the gasifier bed. The charcoal is taken out from the bottom of the bed-section after some residence time at high temperatures to prevent the condensation of tars from the producer gas.

Immediately after ignition of the feedstock inside the downdraft gasifier, the portable syngas analyzer starts recording the volumetric composition and heating value of the gaseous product with a selected time step. Within a few minutes of plant startup, the producer gas starts to form and a flammable gas is typically obtained in less than 15 minutes [30]. After flowing through the gas conditioning unit, where most contaminants and impurities are eliminated, the clean producer gas eventually evacuates through the gas flare stack (unit 9, Fig. 2). At that moment, the gaseous fuel can be flared by using a blowtorch for ignition. During the first minutes of plant operation, the producer gas is typically too rich in tar to be combusted in the internal combustion engine [78]. Therefore, this gaseous fuel with high tar content should be burned off in the flare and purged to the atmosphere until the temperature of the reduction zone has become high enough to produce cleaner producer gas. Steady state conditions are quickly reached in less than one hour [78]. Under steady state operation, the flare must either be colorless or light blue if ignited at night, as long as the tar concentration in the producer is low enough. After several minutes of flare ignition, the inlet valve to the gas engine can be gradually opened, meanwhile to the progressive closing of the gas flare valve. Once the inlet valve is fully open, the gas engine can be cranked and operated until reaching its nominal performance parameters.

The biomass gasification plant should preferably be installed in sheds with all sides open. If the gasifier is to be installed inside any building, the same should be very well ventilated so that no gas accumulation can occur in the event of a leak. A carbon monoxide monitor with an alarm set at about 50 ppm should be placed in the gasifier area and its functioning should be regularly checked. If the concentration of carbon monoxide exceeds 100 ppm (0.01%), the system should be immediately stopped.

2.6. Plant performance evaluation

The primary parameters to be measured for plant performance evaluation were biomass consumption, air and producer gas flow rate, operating temperatures, producer gas composition and Lower Heating Value (LHV), as well as the electrical parameters from the power generation unit.

The recorded values of biomass consumption and air flow rate were used for calculation of the air–fuel equivalence ratio (λ), which is a crucial operating parameter in biomass gasification processes and expresses the actual oxidizer–fuel ratio supplied to the downdraft gasifier in relation to the oxidizer–fuel ratio required for stoichiometric combustion [14, 25, 31, 50, 57, 73, 76].

$$\lambda = \frac{\left(\frac{\dot{m}_{air}}{\dot{m}_f}\right)_{actual}}{\left(\frac{\dot{m}_{air}}{\dot{m}_f}\right)_{stoich}} \tag{5}$$

where $\dot{m}_{air}$ is the mass flow rate of ambient air as gasifying agent and $\dot{m}_f$ is the mass flow rate of exhausted olive pomace pellets as fuel. This definition is the same as that of excess air used for combustion processes, except that it is preferred for air-deficient situations, such as those found in a gasifier [24]. Accordingly, a mixture of air and fuel with $\lambda = 1$ is at stoichiometry; for fuel-rich mixtures, $\lambda < 1$; and for fuel-lean mixtures, $\lambda > 1$. Thus, complete combustion theoretically occurs at an equivalence ratio equal to unity, where all the carbon in the feedstock is stoichiometrically oxidized to provide the maximum concentration of carbon dioxide in the gaseous product stream.

The stoichiometric oxygen requirement was estimated using the average data for the ultimate

analysis of the biomass feedstock reported in Table 1. For a given flow rate of biomass fuel into the downdraft gasifier:

$$\lambda = \frac{(\dot{m}_{O_2})_{actual}}{(\dot{m}_{O_2})_{stoich}} = \frac{(\dot{n}_{O_2})_{actual}}{(\dot{n}_{O_2})_{stoich}} = \frac{y_{O_2,air}\,\dfrac{\dot{m}_{air}}{M_{air}}}{\dot{m}_f\left(\dfrac{x_{C,f}}{M_C} + \dfrac{x_{H,f}}{4\,M_H} - \dfrac{x_{O,f}}{2\,M_O}\right)} \tag{6}$$

where M_{air} is the weighted average molar mass of air, $y_{O_2,air}$ is the mole fraction of oxygen in the atmospheric air and $x_{C,f}$, $x_{H,f}$, $x_{O,f}$ are the mass fractions of carbon, hydrogen and oxygen from the ultimate analysis of the feedstock to the gasification process [64, 90]. The expression in Eq. (6) arises from the complete combustion reaction of a generic solid fuel containing carbon, hydrogen and oxygen, as shown in Eq. (7). Nitrogen and sulfur oxidation reactions were disregarded for calculation of the equivalence ratio, given the comparatively much smaller contents of both elements in the biomass feedstock and the fact that the majority remains bounded to char and tar compounds [22].

$$C_aH_bO_c + \left(a + \frac{b}{4} - \frac{c}{2}\right)O_2 \longrightarrow a\,CO_2 + \frac{b}{2}\,H_2O \tag{7}$$

The lower heating value per unit mass (MJ/kg) of the producer gas can be determined by means of Eq. (8), as a function of the mass fractions (x_i) and lower heating values (LHV_i) of the k fuel components that constitute the clean producer gas (CO, H_2, CH_4 and C_nH_m) [18, 58, 66]. The lower heating values of the major fuel gases at 25 °C are, CO: 10.112 MJ/kg, H_2: 119.96 MJ/kg and CH_4: 50.048 MJ/kg [91].

$$LHV_{cg} = \sum_{i=1}^{k} x_i\,LHV_i \quad (MJ/kg) \tag{8}$$

However, the lower heating value of gaseous fuels such as the producer gas from gasification is typically expressed per unit volume at normal conditions (MJ/Nm^3), as given by Eq. (9).

$$\mathrm{LHV}_{cg} = \sum_{i=1}^{k} y_i \rho_i \mathrm{LHV}_i \quad (\mathrm{MJ/Nm^3}) \tag{9}$$

where y_i and ρ_i are, respectively, the mole fractions and densities at normal temperature and pressure conditions ($T_0 = 0$ °C, $p_0 = 1$ atm) of the k fuel components that constitute the clean producer gas [66, 79]. For calculation of the producer gas density, an ideal gas behavior is assumed [28, 78], such that:

$$\rho_{cg} = \frac{p_{cg} \sum_{i=1}^{k} y_i M_i}{R T_{cg}} \tag{10}$$

where M_i is the molar mass of each gaseous compound. The mass flow rate of producer gas is eventually calculated as given by:

$$\dot{m}_{cg} = \dot{V}_{cg} \rho_{cg} \tag{11}$$

The cold gas efficiency (η_{cg}) is defined as the efficiency of the gasification process after the producer gas has been cleaned up and cooled down to ambient temperature [24]. It expresses the fraction of the chemical energy flow of the biomass feedstock that remains in the cold producer gas. Mathematically, this parameter is determined as follows:

$$\eta_{cg} = \frac{\dot{m}_{cg} \mathrm{LHV}_{cg}}{\dot{m}_f \mathrm{LHV}_f} \tag{12}$$

where $\dot{m}_{cg}$ and $\dot{m}_f$ represent the mass flow rates of cold producer gas and exhausted olive pomace pellets, respectively.

The carbon conversion efficiency (η_{cc}) is defined below as the fraction of solid carbon in the feedstock converted to each of the k gaseous carbon-containing compounds in the clean producer gas (CO, CO_2, CH_4 and C_nH_m) [25, 28, 57, 65, 78],

$$\eta_{cc} = \frac{\dot{V}_{cg}\, p_{cg}}{R\, T_{cg}} \cdot \frac{M_{\mathrm{C}} \sum_{i=1}^{k} y_i\, n_{\mathrm{C}i}}{\dot{m}_f\, x_{\mathrm{C},f}} = \frac{\dot{m}_{cg}\, M_{\mathrm{C}} \sum_{i=1}^{k} \frac{x_i}{M_i}\, n_{\mathrm{C}i}}{\dot{m}_f\, x_{\mathrm{C},f}} \tag{13}$$

where M_{C} is the molar mass of carbon. In addition, $n_{\mathrm{C}i}$ and M_i are, respectively, the number of carbon atoms and molar masses of each carbon-containing compound. For calculation of the carbon conversion efficiency, it is assumed that $\mathrm{C}_n\mathrm{H}_m$ are essentially C_2 hydrocarbons. Also noteworthy is that tar is considered as gas impurity; and hence, not included in the carbon conversion efficiency. If the air–fuel equivalence ratio (λ) is below 0.2, the carbon conversion efficiency decreases drastically [76]. Therefore, in order to maximize the amount of feedstock being gasified, it is advisable that $\lambda > 0.2$.

The power analyzer data include the three-phase active power developed by the wye-connected synchronous generator (P_{gen}), which can be readily determined as given by the following expression:

$$P_{gen} = \sqrt{3}\, U I \cos\varphi \tag{14}$$

where U is the line voltage (V), I is the line current (A) and $\cos\varphi$ is the power factor (PF).

The gross electrical efficiency of the gasification plant ($\eta_{e,gross}$) is calculated according to Eq. (15), as the ratio between the gross electrical power output and the chemical energy flow of the biomass feedstock.

$$\eta_{e,gross} = \frac{P_{gen}}{\dot{m}_f\, \mathrm{LHV}_f} \tag{15}$$

The net electrical efficiency of the gasification plant ($\eta_{e,net}$) is calculated as shown in Eq. (16) by subtracting all the parasitic loads (P_{loads}) from the gross electric power generation [88].

$$\eta_{e,net} = \frac{P_{gen} - P_{loads}}{\dot{m}_f\, \mathrm{LHV}_f} \tag{16}$$

The ratio between the gross electrical efficiency and the cold gas efficiency in Eqs. (15) and (12) indicates the electrical efficiency of the engine–generator set, expressed as follows:

$$\eta_{gen} = \frac{P_{gen}}{\dot{m}_{cg}\,\mathrm{LHV}_{cg}} = \frac{\eta_{e,gross}}{\eta_{cg}} \tag{17}$$

In order to determine the waste heat available in the exhaust gas from the internal combustion engine, the mass flow rate of exhaust gas must be known. The average mass flow rate of exhaust gas for a four-stroke engine can be calculated as shown in Eq. (18). The mass flow rate of an engine depends on the density of ambient air at the intake manifold ($\rho_{air,in}$), the volumetric efficiency (η_V), the engine displacement (V_d), the engine rotational speed (N) and the air/fuel ratio ($m_{cg}/m_{air,in}$) [92].

$$\dot{m}_{eg} = \frac{1}{2}\,\eta_V\,V_d\,N\,\rho_{air,in}\left[1 + \left(\frac{\dot{m}_{cg}}{\dot{m}_{air,in}}\right)\right] \tag{18}$$

2.7. Uncertainty assessment

Uncertainties in the experimental assessment of the gasification plant arise from the accuracy and precision of the measuring instruments, as well as the influence of environmental conditions and observation of the readings [74]. The main uncertainties are associated with the measurements of feedstock consumption and producer gas flow rate [30]. The uncertainties of the different magnitudes were determined following the Guide to the Expression of Uncertainty in Measurement of the International Bureau of Weights and Measures [93]. The feedstock consumption was measured by means of a digital weighting scale with an absolute uncertainty of ±0.1 kg. The pressure drop required in the differential pressure sensor for a specified producer gas flow rate in the Venturi flow meter was measured with an uncertainty of ±0.05 Pa. The uncertainties of the calculated parameters were estimated using the following equation:

$$\Delta f = \sqrt{\left(\frac{\partial f}{\partial z_1}\Delta z_1\right)^2 + \left(\frac{\partial f}{\partial z_2}\Delta z_2\right)^2 + \cdots + \left(\frac{\partial f}{\partial z_n}\Delta z_n\right)^2} \tag{19}$$

where Δf is the uncertainty of the calculated parameter (f) and $z_1, z_2, \ldots, z_n$ are the uncertainties of the measured variables [25, 74, 75]. The uncertainty propagation assessment leads to an uncertainty of approximately 1% in the cold gas efficiency. Other performance parameters such as the gross and net electrical efficiencies exhibit an uncertainty below 0.25%.

3. Results and discussion

This section is structured in four parts. The first part is devoted to investigating the performance of the downdraft gasifier fueled with exhausted olive pomace pellets under steady and transient state operation. The next part examines the performance of the engine–generator set fueled with the producer gas from the gasifier. An overview of the plant performance discussing energy conversion efficiencies and losses is included immediately after. The last part presents an experimental assessment on the rate of production and physicochemical properties of the charcoal discharged from the gasifier.

3.1. Gasifier performance

During operation of the downdraft gasifier fueled with exhausted olive pomace pellets, a rather stable producer gas composition and heating value were attained. Under steady state operation, the LHV of the producer gas essentially ranged between 4.5–5.0 MJ/Nm^3, which is in accordance with the typical range in downdraft fixed bed gasifiers [24]. The average feedstock consumption in the downdraft gasifier was approximately 13.3 kg/h of exhausted olive pomace pellets. The producer gas yield was in the range of 2–3 Nm^3/kg, which is consistent with the typical values reported in the literature [21, 25, 26, 51, 59, 61, 63, 79, 82, 94]. It should be noted that this parameter is determined as the volume of cold producer gas from gasification of each kilogram of feedstock (as received).

Fig. 3 shows the volumetric composition and lower heating value of the producer gas from the downdraft gasifier for 5 hours of continuous operation according to the experimental procedure reported above. The volumetric flow rate of producer gas was adjusted to 40 m^3/h ($\lambda \approx 0.4$)

during the first 150 minutes of operation and then reduced to 30 m^3/h ($\lambda \approx 0.3$) for the remaining 150 minutes. It can be observed that the nitrogen and oxygen concentration drastically decrease during the first 10 minutes of operation as the producer gas begins to form. Nitrogen is virtually inert throughout the gasification process and its concentration in the producer gas declines with the increasing rate of biomass feedstock being gasified. The sharp drop of the oxygen concentration in the producer gas is due to the fact that oxygen is the most reactive component inside the gasifier, followed by steam and carbon dioxide [24]. Initially, the main fuel component in the producer gas is carbon monoxide, because the kinetic rate of the partial oxidation reaction of carbon to form carbon monoxide is the fastest among all the carbon gasification reactions [24]. This reaction quickly consumes the entire oxygen, leaving hardly any for other reactions, and hence, the concentration of carbon monoxide in the producer gas peaks. A comparable trend in the concentration of carbon monoxide during the start-up phase of a downdraft gasifier can be observed in other works [57, 78]. Immediately after, the decreasing concentration of carbon monoxide is mostly explained by the increasing formation of hydrogen and carbon dioxide as a result of the forward water gas shift reaction, which takes place in the gas phase. As a result, the concentration of hydrogen quickly increases at the expense of carbon monoxide. The rapid rate of carbon monoxide formation explains the first peak in the LHV of the producer gas. Worthy of note is that the heating value of carbon monoxide is slightly higher than that of hydrogen if expressed per unit volume. As evidenced in Fig. 3, the concentration of methane also peaks during the start-up phase, which in turn can be related to a higher concentration of tar. For this reason, during the first 30 minutes of plant operation before steady state conditions are reached, the producer gas is usually burned off in the flare stack as a precautionary measure due to the higher tar formation rate in the moments after the gasifier start-up, when the bed temperature is still not high enough. Although tar formation is always an important aspect that must be under control, it did not pose a major issue for plant operation. Indeed, according to manufacturer's specifications, the producer gas conditioning unit is able to reduce the tar content in the cool and clean gas down to around

5–15 mg/Nm^3, which is below the limit value for use as fuel in internal combustion engines (see Table 3). The tar concentration in the conditioned producer gas is measured as indicated in the CEN accredited and approved Technical Specification published by the Energy Research Center of the Netherlands (ECN) [95]. Moreover, it was possible to visually verify in the flare stack that the flame was translucent, practically invisible (light blue if ignited at night), which suggests that the concentration of tar in the producer gas meets the requirements of the engine. Nonetheless, this will have to be confirmed in future works, since tar sampling and detailed analysis is a complex and expensive task that was not planned within the scope of this work.

The steady state is assumed to be reached when thermodynamic equilibrium is virtually attained and there is no significant change in the concentration of the products with time [24]. The time frame required to reach steady state conditions since inception of ignition in the gasifier ranges between 30–60 min. Similar time intervals for reaching steady state conditions have been reported in previous works [21, 31, 78]. Thereafter, very stable volumetric fractions of each gaseous compound are observed. As shown in Fig. 3, the average volumetric composition of the conditioned producer gas formed during steady state operation at a value of $\lambda \approx 0.4$ was: 15.3% CO, 17.7% H_2, 2.3% CH_4, 0.1% C_nH_m, 12.0% CO_2, 0.1% O_2 and 52.5% N_2; whereas during the last 150 minutes of operation at a value of $\lambda \approx 0.3$, the producer gas exhibited the following average volumetric composition: 12.0% CO, 18.1% H_2, 3.2% CH_4, 0.2% C_nH_m, 13.9% CO_2, 0.1% O_2 and 52.5% N_2. It is noteworthy that the plant operator cannot directly modify the value of λ, but the air flow rate across the gasifier bed through adjustment of the butterfly valve. The value of λ was calculated upon termination of the test, as indicated in Eq. (6).

The gasification plant was operating most of the time under steady state conditions. However, at times transient states occur in events such as changing air flow rate, reduced feedstock supply or varying feedstock composition. One of the most effective approaches to controlling the performance of the downdraft gasifier is to modify the air flow rate [35]. This operating parameter allows adjusting the air–fuel equivalence ratio (λ), which indicates the relative air flow rate with respect

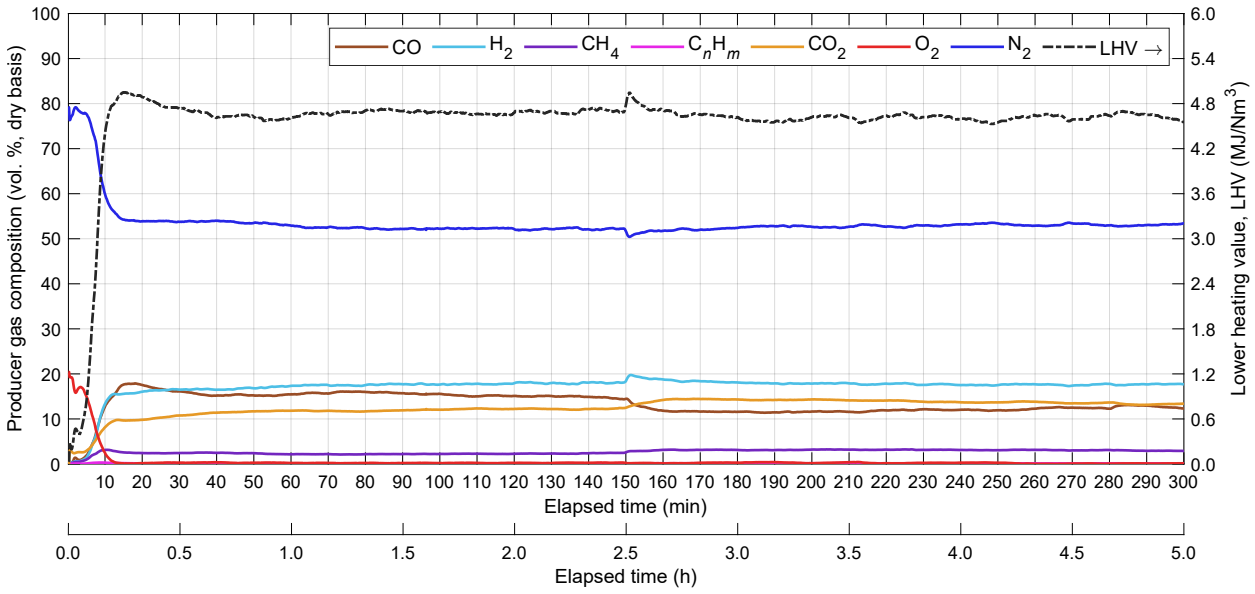

Figure 3: Producer gas composition and heating value for 5 hours of continuous operation.

to the air flow rate required for stoichiometric combustion. The relative air supply plays a key role during the gasification process, as it controls the extent of the exothermic oxidation reactions, which in turn influence the gasification temperature. For higher air flow rates, higher temperatures are reached inside the gasifier, which are conducive to higher carbon conversion efficiencies of the biomass feedstock into producer gas [21]. However, if the air flow rate is too high, an excessive oxidation of the feedstock leads to a substantial reduction in the heating value of the producer gas, and thus, a lower cold gas efficiency [35, 66]. The experimental assessment of the gasifier performance was conducted at varying values of the air–fuel equivalence ratio between 0.2–0.4, which is in full agreement with the typical range for the equivalence ratio in air-blown biomass gasification processes [26, 27, 30, 39, 53, 71, 76]. The pressure drop across the gasifier bed was most of the time in the range of 40–90 mmH_2O (0.39–0.88 kPa), with greater pressure drops occurring under operation at higher values of the equivalence ratio (λ). A comparable differential pressure interval of 50–75 mmH_2O (0.49–0.74 kPa) was reported in a related work [51]. The pressure drop across the producer gas conditioning unit (including the coarse filter, fine filters and safety bag filter), ranged between 20–60 mmH_2O (0.20–0.59 kPa).

The effect of suddenly modifying the air flow rate on the performance of the gasification process can be observed in Fig. 4. In a different run, the volumetric flow rate of producer gas was adjusted to 40 m^3/h until steady state conditions were almost reached in just above one hour of plant operation. Thereafter, the air supply butterfly valve was partially closed to provide a flow rate of 30 m^3/h and then opened again to yield 40 m^3/h at regular intervals of 30 minutes. With increasing air flow rate, the growing availability of oxygen results in lower contents of hydrogen, methane and other light hydrocarbons. Formation of carbon monoxide and water vapor are favored as opposed to carbon dioxide and hydrogen, respectively; as a result of the char and hydrogen oxidation reactions, in addition to the backward water gas shift reaction. The greater availability of oxygen also causes more char to be oxidized to form carbon monoxide, due to the fast kinetics of the partial oxidation reaction, and the CO/CO_2 ratio increases. Furthermore, a higher air flow rate is conducive to higher temperature profiles because of a more pronounced feedstock combustion. Higher temperatures in turn accelerate the Boudouard reaction, promoting higher concentrations of carbon monoxide and lower concentrations of carbon dioxide in the producer gas [69], which also influences the increase in the CO/CO_2 ratio. In addition, an increasing air flow rate leads to a larger presence of nitrogen in the producer gas composition and a reduction in the tar content [66, 69, 86]. By contrast, a decreasing air flow rate is conducive to higher concentrations of hydrogen and light hydrocarbons in the producer gas, while carbon monoxide formation is hindered in favor of carbon dioxide through the forward water gas shift reaction and the CO/CO_2 ratio decreases. A higher amount of methane and light hydrocarbons in a less oxidizing atmosphere also suggests a higher tar production rate [24, 39].

Fig. 5 illustrates the thermal behavior of the downdraft gasifier during operation under steady state conditions. Surface temperatures were continuously monitored along the gasifier height by means of a thermographic camera (SATIR D600, Ireland). The maximum temperature on the external surface of the gasifier was between 350–400 °C, while the minimum temperature shown in the thermogram corresponds to the ambient temperature. However, it is noteworthy that the ther-

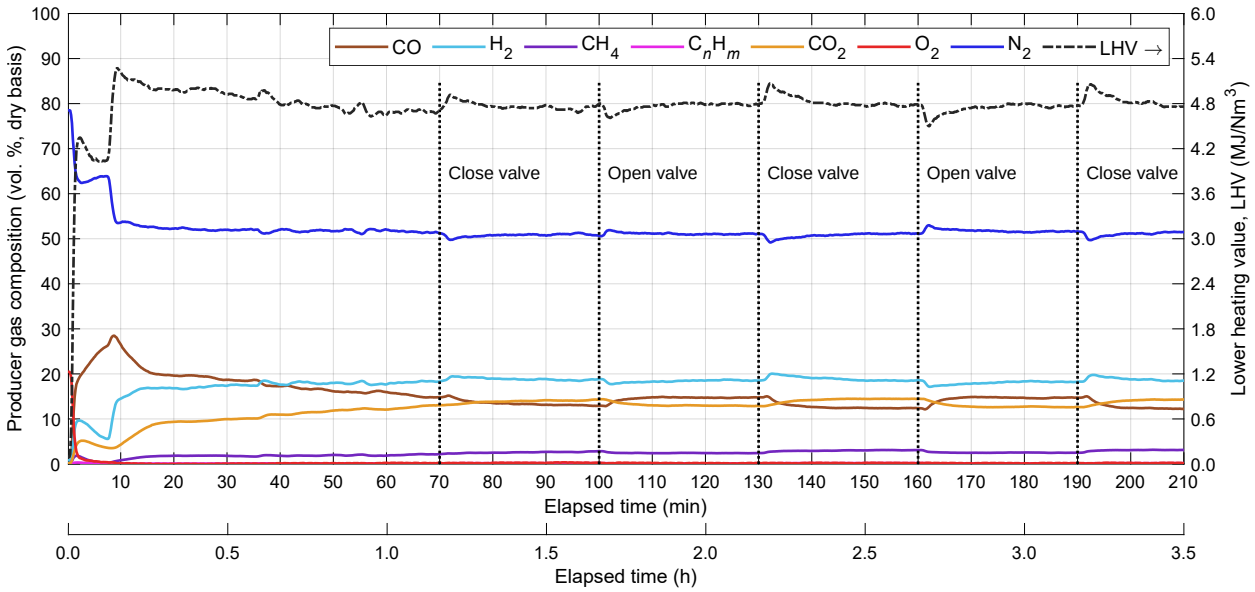

Figure 4: Effect of modifying the air flow rate on the producer gas composition and heating value.

mogram is included in this work for the purpose of graphically showing the relative distribution of temperatures in the gasifier, rather than the specific values of surface temperatures. In this regard, a stratified temperature distribution is clearly observed along the vertical axis of the gasifier, where the drying, pyrolysis, oxidation and reduction zones can be identified. As indicated by the thermocouple readings, the maximum temperature in the oxidation zone was observed to lie most of time within 800–1100 °C [21, 57, 58, 67, 76], with average maximum temperatures around 1000 °C when the gasifier is operating under steady state conditions [26, 35]. The high maximum temperatures reached inside the gasifier promote tar cracking, which is reported to occur at temperatures between 700 and 1250 °C [28]. The subsequent temperature decrease just below the oxidation zone is attributed to the endothermic reactions taking place in the reduction zone and leading to the formation of the fuel gases in the producer gas [76].

3.2. Engine and generator performance

The producer gas from gasification, once conditioned, is eventually used as fuel in a reciprocating gas engine coupled to an electric generator. The chemical energy of the cold producer gas is ultimately converted into four forms of energy in the engine–generator set: shaft work for

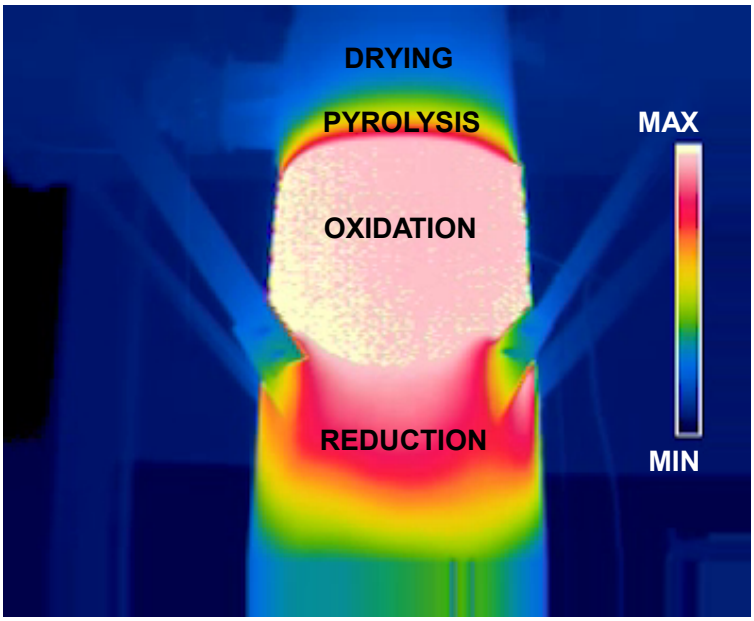

Figure 5: Thermogram of the downdraft gasifier under steady state operation showing a stratified temperature distribution. The maximum temperature is 350–400 °C, while the minimum temperature corresponds to ambient temperature.

electricity generation, exhaust gas as high-temperature waste heat, jacket cooling water as low-temperature waste heat, and unrecoverable heat losses [58].

The efficiency of electric generators driven by reciprocating internal combustion engines in small-scale units is usually in the range of 30–35%, but in the context of low-grade fuel gases such as producer gas, their efficiency is lowered significantly [19, 96]. The theoretical value of power derating when a natural gas engine is switched to operate on producer gas is about 30% [26, 85]. Engine power derating when using producer gas as fuel can be as high as 70% [97], although this power drop can be compensated by the reduction in emissions of greenhouse gases and other pollutants [97]. The reduction in power of an engine operated with producer gas is mainly attributed to the lower heating value of the fuel, in addition to the high volume of gas/air mixture that enters the engine cylinders, namely the volumetric efficiency, which limits the engine power [85].

The electrical power output from the generator was dissipated as heat by means of a resistive load bank [38, 58, 59, 78], made up of 10 heating elements connected in parallel so as to draw the

maximum power from the generator on each of the three phases. Fig. 6 shows an electrical wiring diagram for connection of the resistive load bank to the output of the wye-connected three-phase generator, where specific colors are used for identification of common neutral and AC phase conductors according to international standard IEC 60446. Each resistor has a minimum load interval of ~0.6 kW and a maximum power consumption of ~1.2 kW. Increasing the load slowly with increments of 0.6–3.6 kW and adjusting the intake butterfly valve allowed to maintain the engine at a stable operation [58]. When the engine–generator set becomes overloaded, the gross electrical power output drops below 50 Hz or 230 V, and the system is shut down [58]. Several operational configurations were tested under part-load and full-load operation, with electrical power outputs ranging between 3.6–12.0 kW [78]. The line current under operation near its power rating was measured to 15.2 A and the total power dissipated as heat by the heating elements in the three phases was 10.5 kW. The maximum electrical power output from the engine–generator set under full load operation when fueled with the producer gas from gasification of exhausted olive pomace pellets was about 12 kW, which is ~2 kW above its power rating. This proves that the producer gas from gasification of exhausted olive pomace pellets was able to drive the engine–generator set to its full power rating. However, operation close to the design point is recommended to prevent potential damages to the electromechanical equipment. The gross electric power generated from the constant 400 V line to line voltages arranged in wye connection was maintained for almost all the time at a desired constant frequency of 50 Hz, with the engine crankshaft rotating at a speed of 1500 rpm. The minimum and maximum values for the frequency during transient states were 49.35 Hz and 50.79 Hz, respectively; thus, complying with the required range of 49.0–51.0 Hz for connection to the national electricity grid [98]. The power factor ($\cos\varphi$) and total harmonic distortion (THD) are other key quality indicators of the electrical power output. In a high-quality power generation unit, $\cos\varphi$ should be as close to one as possible and THD should be as low as possible. That was the case of the electrical power output from the engine–generator set, since $\cos\varphi$ was very close to unity and THD was always below 1%.

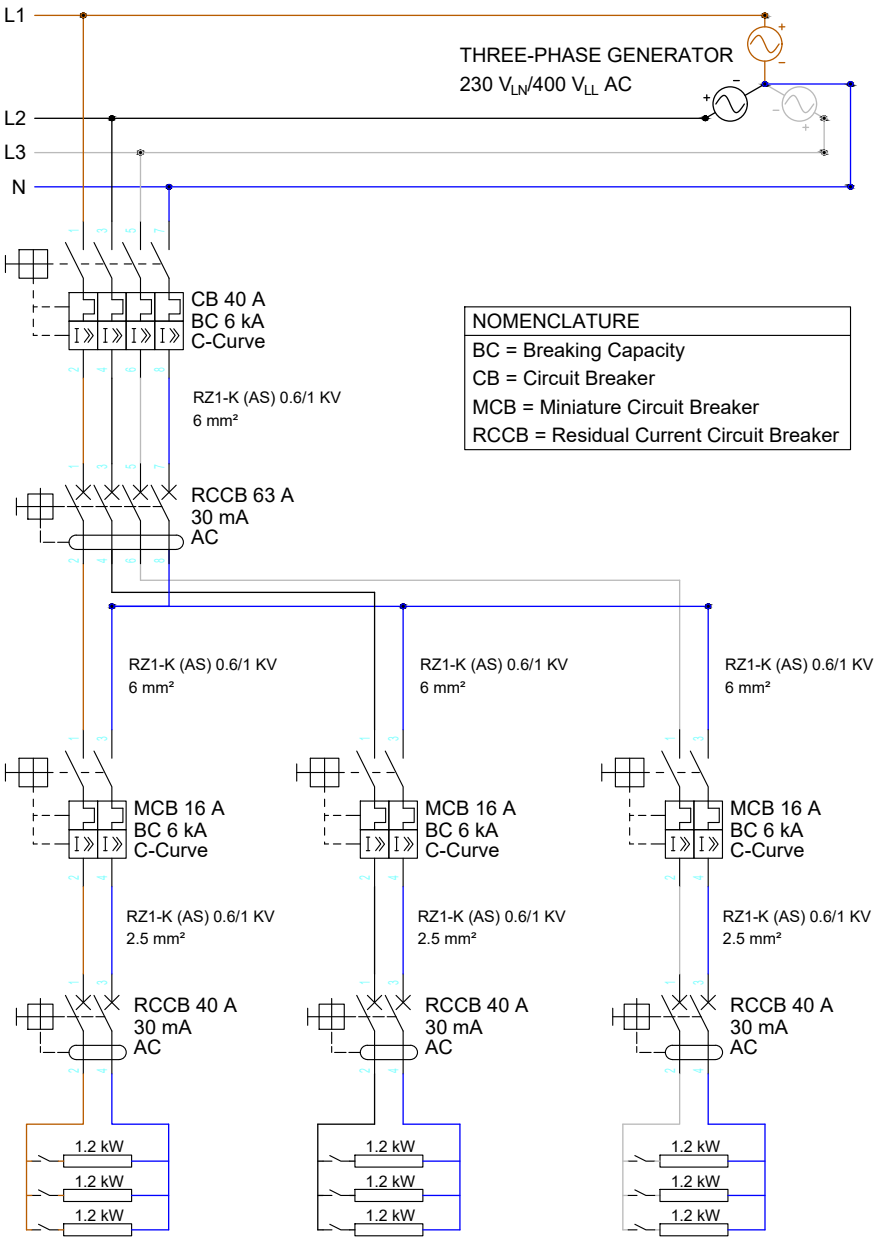

Figure 6: Electrical wiring diagram for connection of the three-phase generator to a resistive load bank.

An example of the electrical performance of the gasification plant during 5 hours of continuous operation is presented in Fig. 7. The electrical power output of the engine–generator set was evaluated under purely resistive step loads of 3.6, 7.2 and 10.8 kW, or roughly 1/3, 2/3 and 3/3 of the nominal operating conditions. The maximum power output was established as 10.8 kW, which lies within the 10% tolerance interval on the nominal value, because an additional load

increment beyond this value for a prolonged period could eventually damage the electric generator. The load was adjusted by suddenly turning on each of the 1.2 kW heating elements connected to each of the three phases, so as to achieve a balanced load. However, to prevent the electric generator from shutting down in near-nominal operation with large load increments (i.e., 3.6 kW), the load increase was staggered in smaller 0.6 kW increments on each of the three phases, as indicated in Fig. 7 just before 200 minutes of operation. The three-phase load becomes unbalanced in that short period of load adjustment time. As evidenced in Fig. 7, the actual resistive load of each heating element was slightly below their rated value, and thus, the measured resistive step loads were 3.5, 7.0 and 10.5 kW. Worthy of note is the difference between the electrical power output from the generator and the net electrical power output after all parasitic loads have been subtracted. The main sources of own electrical consumption are the ancillary components, especially the electric motors. The power drawn by the parasitic loads was in the range of 1.5–2.5 kW, which represents about 15–25% of the gross electrical power output under nominal operating conditions. The graph in Fig. 7 also shows the gross electricity production in the generator, as well as the net electricity production and consumption of the gasification plant over the 5-hour operational timeframe. It takes approximately 20–30 minutes to start the gasification plant from cold state to the beginning of electricity production. The gasification plant gets into a positive balance of electricity production in another 20–30 minutes. After the nominal power output of the generator is achieved, a relatively fast increase of the net electricity generation follows. The whole gasification plant is rather robust, largely due to the large thermal inertia of the downdraft gasifier. This robustness is advantageous under nominal conditions to maintain a stable operation at the expense of flexibility. Notwithstanding the benefits of operation under the rated power output, at times it is possible to maintain the gasification plant under part-load operation. The specific feedstock consumption, however, increases if the gasification plant is operated at partial load [51], with values between 1.3–3.8 kg of biomass (as received) per kWh of gross electrical output. This is because with increasing electric power loads, the flow rate of producer gas increases

substantially, while its lower heating value decreases slightly [78]. Comparable values for the specific feedstock consumption have been reported in the literature [21, 55, 59, 68, 82]. The specific feedstock consumption achieved under nominal operating conditions was 1.3 kg/kWh. This value is very close to the specific feedstock consumption of 1.2 kg/kWh reported for a similar biomass gasification plant from a different manufacturer, which was fueled with cotton residues [42].

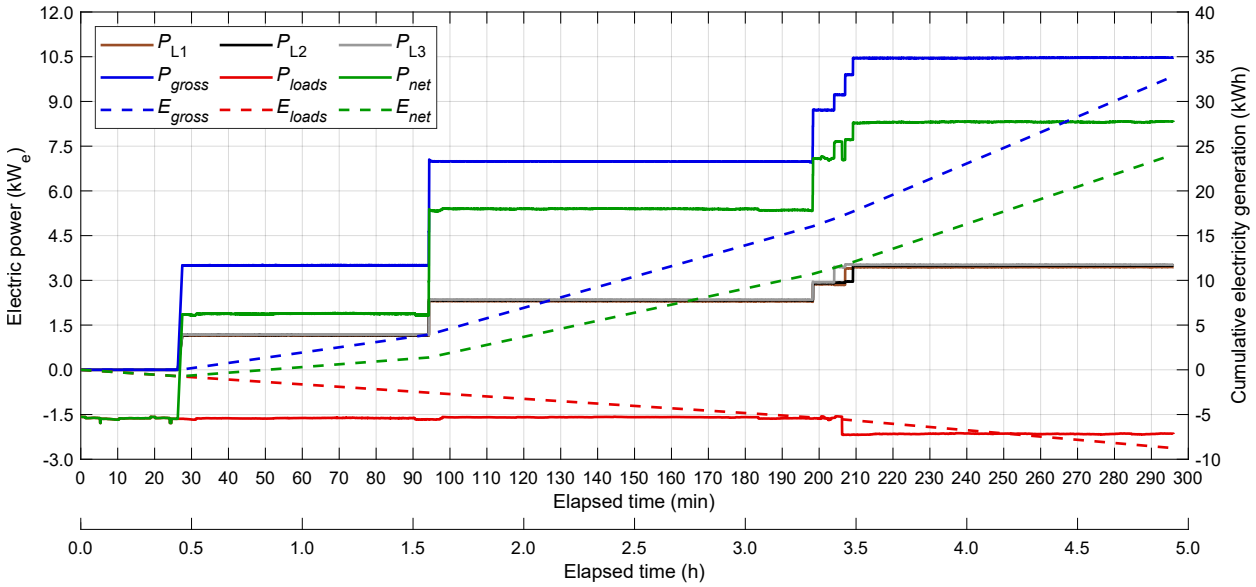

Figure 7: Electricity production and consumption of the gasification plant for 5 hours of continuous operation at varying electric power loads.

An effective use of the available thermal energy contained in the jacket cooling water and exhaust gas can improve the economics of the gasification plant. Cooling system heat and exhaust heat are typically recovered in roughly equal proportions from a gas engine CHP unit. However, compared to compression-ignition (diesel) engines, spark-ignition engines give up less heat to the exhaust gases, and thus, more heat to the cooling system, as they operate with less excess air [99]. The high-temperature heat source is the engine exhaust, at 350–450 °C; whereas the jacket water leaves the engine at about 85–90 °C. A minor amount of low-grade heat could also be recovered from the engine lube oil [67]. The recovered waste heat from the exhaust gas and cooling systems can be used to meet the thermal energy needs of the olive oil production process in the oil mill.

The available high-temperature heat in the exhaust gas was estimated at about 9 kW_{th}, as a function of the flow rate of exhaust gas and the average temperature at the engine exhaust [66, 100]. The mass flow rate of exhaust gas was calculated through Eq. (16), considering an excess air coefficient of $\lambda \approx 1.05$ [21, 64, 85, 97, 100], which is obtained from an oxygen lambda probe placed at the end of the exhaust gas pipe. The composition of the exhaust gas is obtained through mass balance from the complete combustion equation of the producer gas with such excess air [66]. The mass heat capacity (c_p) of the exhaust gas at constant pressure was determined as a function of the percentage in mass of each component in the mixture [67, 68]. Under nominal operating conditions, an average exhaust temperature close to 400 °C was measured with a K-type thermocouple. It is worth noting that, even though the electricity generation efficiency of engine–generator sets typically increases with size, smaller engines often have a higher exhaust gas temperature than larger engines [99].

A closed cooling water circuit is used to cool the engine. The available low-temperature heat in the jacket cooling water was estimated for the nominal condition as a function of the flow rate of cooling water, and the temperatures at the supply and return lines of the cooling system [66, 100]. The temperature of the engine cooling water was maintained in the range of 70–90 °C. The recovered heat could be used to produce hot water for the two-phase olive oil extraction process in the oil mill.

3.3. Overall plant performance

The same example of 5-hour plant operation from the previous section is used to examine the overall performance of the gasification plant. After half an hour of plant operation from inception of ignition of the gasifier to the beginning of electricity generation, the process efficiencies during the remaining 4.5 hours of operation are presented in Fig. 8. The gasification plant was operating under increasing step loads of roughly 1/3, 2/3 and 3/3 of the nominal operating conditions.

The cold gas efficiency (η_{cg}) ranged from around 50% under low-load operation to roughly 70% under nominal operating conditions. This means that at least 30% of the chemical energy

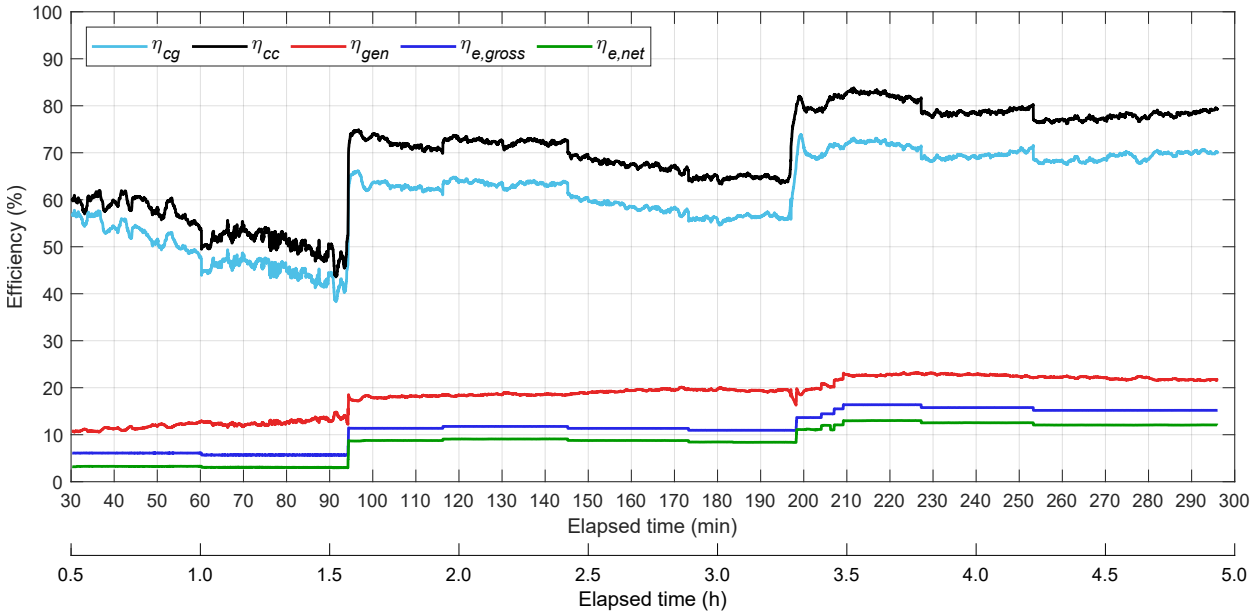

Figure 8: Different conversion efficiencies in the gasification plant for 5 hours of continuous operation at varying electric power loads.

contained in the biomass feedstock is lost to the environment. In other words, a maximum of about 70% of the chemical energy contained in the exhausted olive pomace pellets is preserved in the producer gas. The interval 50–70% is consistent with the typical range reported for the cold gas efficiency in downdraft gasifiers [25, 26, 35, 50, 51, 66, 68, 94]. The cold gas efficiency also decreases under operation at reduced load, as suggested in previous works [21, 50]. The average cold gas efficiency under nominal operating conditions was 69.8%, which is in accordance with the average cold gas efficiency reported for similar biomass gasification systems from different manufacturers [35, 39, 50, 51, 61, 71, 78, 94].

The carbon conversion efficiency (η_{cc}) of the biomass feedstock into producer gas follows a similar trend to the cold gas efficiency. Under part-load operation, the carbon conversion efficiency is smaller, thus favoring charcoal production. By contrast, the carbon conversion efficiency under nominal operating conditions reaches just above 80%, which indicates that most of the carbon in the biomass feedstock is being gasified, with only around 20% by weight discharged from the bottom of the gasifier as charcoal. The maximum carbon conversion efficiency achieved in this

work was 83.83%, which is in very good agreement with the maximum value of 83.15% reported for the carbon conversion efficiency in a related experimental work [78]. Unlike carbon, most of the nitrogen, sulfur and chlorine content of the biomass feedstock appears to remain bounded to char and tar compounds. For example, although not directly measured, the mass balance indicates that the amount of sulfur-containing compounds in the producer gas is expected to be negligible, representing less than 0.01% by weight of the conditioned producer gas stream. Similar conclusions can be reached for the mass balances of nitrogen and chlorine, which agrees with the findings of previous works [22].

The electrical efficiency of the engine–generator set (η_{gen}) determines the gross electrical output of the generator in relation to the chemical energy of the producer gas supplied to the gas engine. This parameter ranged from around 10% under minimum load operation to 21–23% under nominal operating conditions. Comparable gross electricity generation efficiencies of spark-ignition engine–generator sets powered by producer gas from biomass gasification are reported in previous experimental and simulation works [15, 18, 67, 68], while another related work reported efficiencies in the range of 25.6–29.5% for the spark-ignition engine alone [58], assuming an electrical efficiency of the generator equal to 95%. These comparisons are reasonable, as the electrical efficiency typically decreases with the size of the engine–generator set.

The gross electrical efficiency ($\eta_{e,gross}$) and net electrical efficiency ($\eta_{e,net}$) follow a similar trend to the rest of energy conversion efficiencies, with lower values attained under part-load operation. All these findings are in good agreement with other works in the scientific literature, which also concluded that energy conversion efficiencies typically decrease under part-load operation and increase when the system is operating under nominal conditions [21, 50, 51]. Under nominal operation, the gross and net electrical efficiencies of the gasification plant are 15–17% and 12–13%, respectively. Worthy of note is the high relative difference between the gross and net electrical efficiencies, especially under part-load operation. This is due to the nearly constant power drawn by the parasitic loads, which may account for up to half of the gross electricity generation under

1/3 of nominal load operation. The parasitic electricity consumption under nominal load operation is close to 20% of the gross electrical output. Somewhat lower values in the range of 15.9–17.6% have been reported for the share of auxiliary electricity self-consumption in larger gasification plants [88]. Accordingly, the net electrical efficiency achieved in this work would still have certain room for improvement in a scaled-up gasification plant, as a result of an expected relatively lower share of parasitic loads.

In order to provide an overview of the energy flows and losses, Fig. 9 illustrates the overall energy balance of the gasification plant under nominal load operation in the form of a Sankey diagram. As evidenced in the energy balance, approximately 15.9% of the input chemical energy in the biomass feedstock to the downdraft gasifier is converted into gross electric power. The remaining 84.1% of the energy flow represents available thermal energy from the gas engine (31.8%) and unrecoverable waste heat as thermal losses to the environment (54.0%). Most of the unrecoverable heat losses are originated in the downdraft gasifier and producer gas conditioning unit, while other significant power conversion losses as low-grade waste heat occur in the engine generator set. In this regard, other previous works have also concluded that the gasification process and producer gas conditioning take up the largest share among all energy losses [64, 66, 88]. Heat transfer though the gasifier walls, discharge of hot solids (charcoal) and wet scrubbing of the producer gas are the main sources of energy loss during the gasification process and producer gas conditioning. A substantial amount of waste heat is recoverable from the exhaust gas and jacket cooling water, which respectively represent 14.3% and 17.5% of the input energy flow; whereas the remaining 23.8% corresponds to unrecoverable low-grade waste heat, including convective and radiation losses, friction, power conversion losses, etc. These unrecoverable heat losses typically increase in case of low-load operation of the internal combustion engine [64]. Electricity consumption by the ancillary equipment included in the balance of plant is estimated at around 20% of the gross electric power generation from the engine–generator set. As a result, the net electrical power output of the gasification plant is estimated at about 12.7% of the input energy flow. This value for

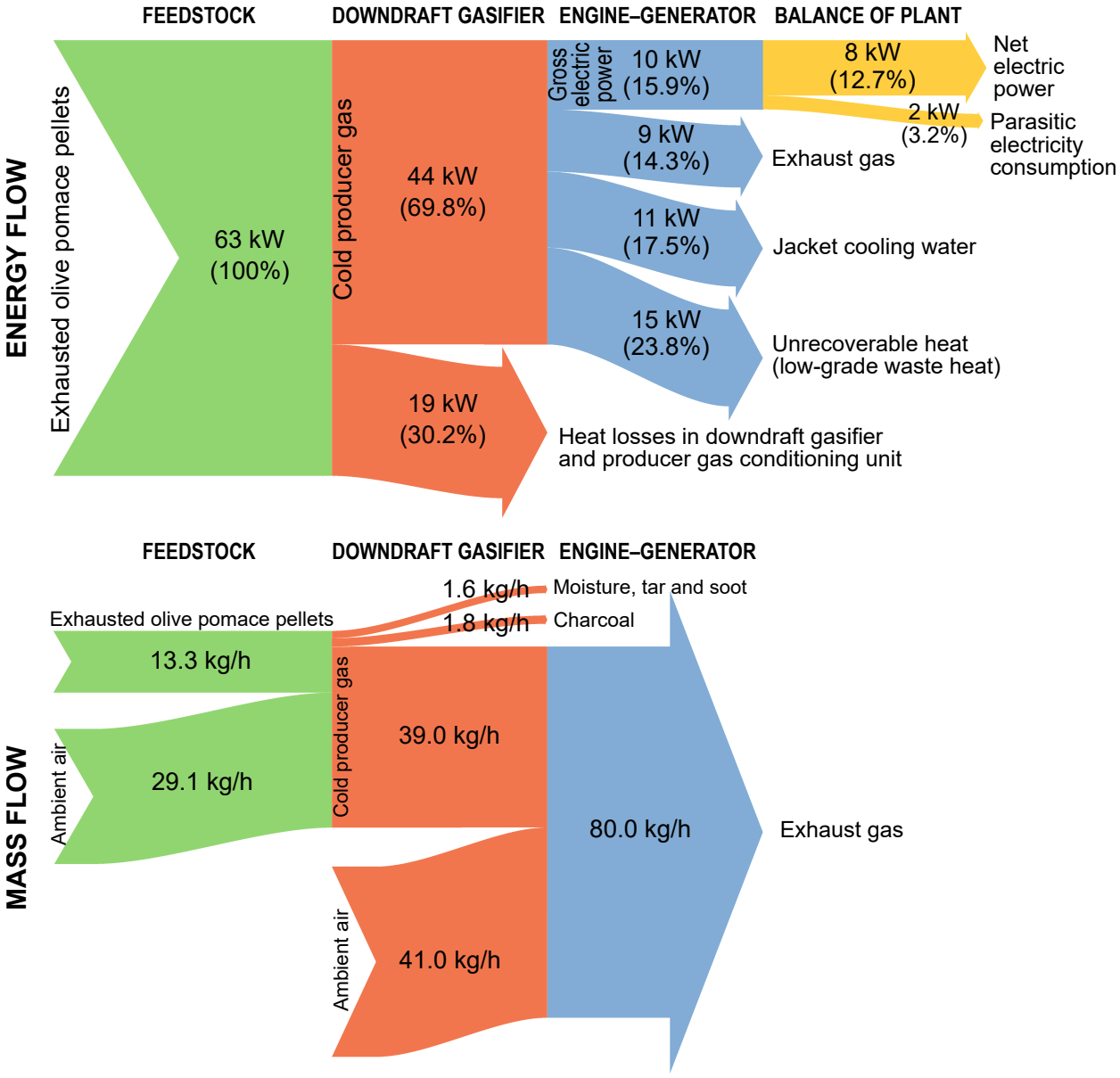

Figure 9: Energy and mass flow diagrams of the gasification plant under nominal operating conditions.

the net electrical efficiency is consistent with the values reported in previous works [51, 94]. A comparative distribution of the energy flows and losses for a similar gasification plant fueled with olive pits and tree pruning is provided in [18].

As a complement to the energy balance, a mass balance diagram of the gasification plant is also provided in Fig. 9 for the steady state condition. The average consumption of exhausted olive

pomace pellets in the downdraft gasifier is 13.3 kg/h, which constitutes an average chemical energy input of approximately 63 kW. This value for the feedstock consumption corresponds to eleven batches of exhausted olive pomace pellets of 6 kg each (66 kg in total) in just under five hours of continuous operation. Under nominal operating conditions, the flow rate of conditioned producer gas is 39.0 kg/h, which contributes to about 44 kW of the energy flow. The calculated flow rate of air through nitrogen balance is 29.1 kg/h, which gives an air–fuel equivalence ratio of $\lambda \approx 0.37$. On the other hand, the measured average charcoal production is 1.8 kg/h. The remaining 1.6 kg/h in the mass balance of gasification and producer gas conditioning are attributed to moisture, tar and soot removal in the producer gas conditioning unit. Finally, as the engine operates with an excess air coefficient of $\lambda \approx 1.05$, the flow rate of air at the intake manifold is 41.0 kg/h, which, together with the producer gas, eventually forms the exhaust gas stream leaving the engine at a flow rate of 80.0 kg/h.

3.4. Biochar production

In addition to useful thermal and electrical energy, the pilot-scale gasification plant produces a valuable carbonaceous solid material known as biochar. In fact, the major advantage of gasification over carbonization or pyrolysis is the combined production of electricity, heat and biochar [36, 42]. The average biochar production rate was quantified by weighing the charcoal accumulated in the collection box below the gasifier grate [72]. The charcoal was previously air-dried until a moisture content close to 10% (wet basis) was reached. A picture of an air-dried charcoal sample (as received) is shown in Fig. 10. The average production rate of air-dried charcoal from the downdraft gasifier under steady state operation was 1.8±0.2 kg/h, or about 12–15% by weight of the input biomass feedstock (as received). This value matches with the estimated charcoal production through carbon balance from the measured feedstock consumption and the calculated carbon conversion efficiency.

A sample of the charcoal produced during the gasification process of exhausted olive pomace pellets was collected and physicochemically characterized in an external test laboratory. The char-

Figure 10: Charcoal from gasification of exhausted olive pomace pellets in a downdraft gasifier.

acterization report includes the proximate and ultimate analyses, bulk density and specific surface area. The main results from the analyzed sample are listed in Table 4. High-value biochars are typically characterized by high carbon content, low H/C and O/C molar ratios, low ash content, high surface area, high conductivity and high ion exchange capacity, with low levels of contaminants [47]. As required by the IBI and EBC definitions of biochar, the carbonaceous solid material discharged from the downdraft gasifier exhibits molar ratios of $H/C < 0.7$, and $O/C < 0.4$. In addition, the total content of carbon was ≥ 50 wt.% on a dry basis, as indicated in the EBC certification standard [49]. No limits yet exist on other parameters such as bulk density, specific surface area, porosity and water holding capacity [48]. As expected, the charcoal discharged from the downdraft gasifier generally showed low bulk density. In terms of the specific surface area, no minimum values are specified, but the EBC certification standard states that this parameter should preferably be higher than 150 $m^2 \cdot g^{-1}$ [47], as is the case with the charcoal from gasification of exhausted olive pomace pellets. Nonetheless, further analyses must be performed to certify the environmental and health safety of this carbonaceous solid by-product from gasification for agronomic use. Both the IBI and EBC certification standards impose strict limits on some hazardous pollutants such as heavy metals, PAHs, PCBs, dioxins and furans [47–49]. In particular, the 16 polycyclic aromatic hydrocarbons classified by the Environmental Protection Agency (EPA) of the United States as priority contaminants are the most critical to be measured [48]. The thresholds

for each specific property set by both certification standards can be consulted in [47, 49].

Table 4: Physicochemical properties of charcoal from gasification of exhausted olive pomace pellets.

Parameter	**Value**	**Unit**	**Standard method**
Moisture content	10.5 ± 0.1	wt.% as received	ISO 18134:2015
Ash content (550±10 °C)	21.9 ± 0.1	wt.% dry basis	ISO 18122:2015
Carbon (C), total	69.5 ± 0.2	wt.% dry basis	ISO 16948:2015
Hydrogen (H), total	0.8 ± 0.1	wt.% dry basis	ISO 16948:2015
Nitrogen (N), total	1.54 ± 0.05	wt.% dry basis	ISO 16948:2015
Sulfur (S), total	0.34 ± 0.03	wt.% dry basis	ISO 16948:2015
Oxygen (O), total	5.9	wt.% dry basis	Calculated
H/C ratio	0.137	Molar dry basis	Calculated
O/C ratio	0.064	Molar dry basis	Calculated
Bulk density	363	kg/m^3	ISO 17828:2015
Specific surface area (BET)	199.7	m^2/g	ISO 9277:2009

4. Conclusions and future works

The present work has demonstrated the technical feasibility of gasifying exhausted olive pomace pellets for combined production of electricity, heat and biochar on a distributed scale in the olive oil industry. To this end, a pilot-scale gasification plant consisting of an air-blown downdraft fixed-bed gasifier, a producer gas conditioning unit and a four-stroke spark-ignition engine coupled to an electric generator was installed in the proximity of an olive oil mill. As far as the authors are aware, the pilot-scale gasification plant that has been tested in this work is the first of its kind to be fed with olive pomace. An extensive experimental assessment of this facility was performed under partial and nominal load operation and was supplemented by a physicochemical analysis of the carbonaceous solid material discharged from the gasifier. Dynamic plant performance data is also provided, the availability of which in the scientific literature is rather scarce. Real-time measurements of diverse performance parameters confirmed a remarkably good and reliable operability of the gasification plant. The producer gas quickly reached a steady composition and heating value (4.5–5.0 MJ/Nm^3) in less than one hour since inception of feedstock ignition inside the gasifier, while the engine–generator set was able to adapt to varying loads and still provide a stable electrical power output. The specific feedstock consumption, however, increased when

the gasification plant was operated at partial load, with values between 1.3–3.8 kg of biomass (as received) per kWh of gross electrical output. Under nominal operating conditions, the gasification plant achieved a net electrical efficiency of 12–13%, with an average carbon conversion efficiency of the biomass feedstock into producer gas just above 80% and an average cold gas efficiency close to 70%. The average production rate of air-dried charcoal from the downdraft gasifier was about 12–15% by weight of the input biomass feedstock (as received). The physicochemical analysis of the charcoal discharged from the gasifier revealed advantageous properties for agronomic use.

Gasification of olive pomace for the concurrent production of renewable electricity, heat and biochar represents a promising opportunity to foster the circular economy in the olive oil industry. Nevertheless, a major limitation of the pilot-scale gasification plant subject of this work resides in its relatively reduced size, which makes it versatile for research, but restricts its profitability. Accordingly, future research works will be aimed at developing a scaled-up biomass gasification plant with better prospects for commercialization in the olive oil sector.

Nomenclature

Symbols

d	Diameter [m]
I	Current [A]
m	Mass [kg]
$\dot{m}$	Mass flow rate [kg·s^{-1}]
M	Molar mass [kg·kmol^{-1}]
n	Number of atoms
N	Rotational speed [s^{-1}]
p	Pressure [kPa]
P	Power [kW]
R	Gas constant [kJ·kmol^{-1}·K^{-1}]

t Time [s]

T Temperature [K]

U Voltage [V]

V Volume [m^3]

$\dot{V}$ Volume flow rate [$m^3 \cdot s^{-1}$]

x Mass fraction

y Mole fraction

Greek letters

η Efficiency

λ Air–fuel equivalence ratio

ρ Density [$kg \cdot m^{-3}$]

φ Phase angle between current and voltage

Subscripts

air Ambient air

cc Carbon conversion

cg Cold producer gas

d Displacement

e Electricity

eg Exhaust gas

f Feedstock or fuel

gen Engine–generator set

$loads$ Parasitic loads

Abbreviations

AC Alternating current

AVR Automatic voltage regulator

BOP Balance of plant

CHP Combined heat and power

FS Full scale

HHV Higher heating value

LHV Lower heating value

PAH Polycyclic aromatic hydrocarbon

PCB Polychlorinated biphenyl

PF Power factor

THD Total harmonic distortion

CRediT authorship contribution statement

R. Aguado: Conceptualization, Formal analysis, Investigation, Methodology, Validation, Visualization, Writing - Original Draft, Writing - Review & Editing. **A. Escámez:** Data curation, Investigation, Methodology, Resources, Software. **F. Jurado:** Funding acquisition, Resources, Supervision. **D. Vera:** Conceptualization, Funding acquisition, Investigation, Methodology, Project administration, Supervision, Validation.

Declaration of competing interest

The authors declare no known personal or financial competing interest.

Acknowledgements

The authors deeply appreciate the technical support and assistance provided by IFAPA Centro "Venta del Llano" (*Junta de Andalucía*).

Funding

This research work was supported by the project entitled "Hacia una producción sostenible y sin residuos en la industria oleícola: un modelo de economía circular" (Ref. No. 1381442), co-funded by *Programa Operativo FEDER 2014–2020* and *Consejería de Economía y Conocimiento de la Junta de Andalucía* of the Spanish Government.

Roque Aguado gratefully acknowledges financial support from *Ministerio de Universidades* under the FPU Program (Ref. FPU19/00930).

References

[1] Economic Affairs & Promotion Unit - International Olive Council (IOC), https://www.internationaloliveoil.org/what-we-do/economic-affairs-promotion-unit/, Accessed: 2022-06-18.

[2] Food and Agriculture Organization of the United Nations, Statistics Division (FAOSTAT), http://www.fao.org/faostat/en/, Accessed: 2022-06-18.

[3] S. I. Patsios, K. N. Kontogiannopoulos, G. F. Banias, Environmental impact assessment in agri-production, in: Bio-Economy and Agri-production, Elsevier, 2021, pp. 83–116. doi:10.1016/b978-0-12-819774-5.00005-9.

[4] Junta de Andalucía, Consejería de Agricultura y Pesca, Plan Director del Olivar Andaluz, https://www.juntadeandalucia.es/organismos/transparencia/planificacion-evaluacion-estadistica/planes/detalle/59239.html (2015).

[5] J. Rodríguez-Cohard, J. Sánchez-Martínez, V. Gallego-Simón, Olive crops and rural development: Capital, knowledge and tradition, Reg. Sci. Policy Pract. 11 (6) (2018) 935–949. doi:10.1111/rsp3.12115.

[6] A. G. Pantziaros, X. A. Trachili, A. D. Zentelis, V. Sygouni, C. A. Paraskeva, A new olive oil production scheme with almost zero wastes, Biomass Conv. Bioref. 11 (2021) 547–557. doi:10.1007/s13399-020-00625-0.

[7] Regional Activity Centre for Cleaner Production (RAC/CP). Pollution prevention in olive oil production, Available at: http://www.cprac.org/docs/Olive20Oil20Production.pdf, Accessed: 2022-06-18.

[8] R. Arjona, A. García, P. Ollero, The drying of alpeorujo, a waste product of the olive oil mill industry, J. Food Eng. 41 (3) (1999) 229–234. doi:10.1016/S0260-8774(99)00104-1.

[9] C. Sánchez-Sánchez, A. González-González, F. Cuadros-Salcedo, F. Cuadros-Blázquez, Two-phase olive mill

waste: A circular economy solution to an imminent problem in Southern Europe, J. Clean. Prod. 274 (2020) 122789. doi:10.1016/j.jclepro.2020.122789.

[10] A. García-Maraver, M. Zamorano, A. Ramos-Ridao, L. Díaz, Analysis of olive grove residual biomass potential for electric and thermal energy generation in Andalusia (Spain), Renew. Sust. Energ. Rev. 16 (1) (2012) 745–751. doi:10.1016/j.rser.2011.08.040.

[11] Agencia Andaluza de la Energía, La bioenergía en Andalucía, https://www.agenciaandaluzadelaenergia.es/sites/default/files/Documentos/3_2_0068_20_LA_BIOENERGIA_EN_ANDALUCIA.PDF, Accessed: 2022-06-18 (2020).

[12] Instituto para la Diversificación y Ahorro de la Energía (IDAE), Informe de Precios de la Biomasa para Usos Térmicos, https://www.idae.es/informacion-y-publicaciones/estudios-informes-y-estadisticas, Accessed: 2022-06-18 (2020).

[13] V. Skoulou, A. Zabaniotou, G. Stavropoulos, G. Sakelaropoulos, Syngas production from olive tree cuttings and olive kernels in a downdraft fixed-bed gasifier, Int. J. Hydrog. Energy 33 (4) (2008) 1185–1194. doi:10.1016/j.ijhydene.2007.12.051.

[14] D. Vera, F. Jurado, K. D. Panopoulos, P. Grammelis, Modelling of biomass gasifier and microturbine for the olive oil industry, Int. J. Energy Res. 36 (3) (2012) 355–367. doi:10.1002/er.1802.

[15] D. Vera, B. de Mena, F. Jurado, G. Schories, Study of a downdraft gasifier and gas engine fueled with olive oil industry wastes, Appl. Therm. Eng. 51 (1) (2013) 119–129. doi:10.1016/j.applthermaleng.2012.09.012.

[16] M. Dogru, Experimental results of olive pits gasification in a fixed bed downdraft gasifier system, Int. J. Green Energy 10 (4) (2013) 348–361. doi:10.1080/15435075.2012.655351.

[17] A. Zabaniotou, P. Mitsakis, D. Mertzis, S. Tsiakmakis, P. Manara, Z. Samaras, Bioenergy technology: Gasification with internal combustion engine application, Energy Procedia 42 (2013) 745–753. doi:10.1016/j.egypro.2013.11.077.

[18] D. Vera, F. Jurado, N. K. Margaritis, P. Grammelis, Experimental and economic study of a gasification plant fuelled with olive industry wastes, Energy Sustain. Dev. 23 (2014) 247–257. doi:10.1016/j.esd.2014.09.011.

[19] F. Y. Hagos, A. R. A. Aziz, S. A. Sulaiman, Trends of syngas as a fuel in internal combustion engines, Adv. Mech. Eng. 6 (2014) 401587. doi:10.1155/2014/401587.

[20] M. Formica, S. Frigo, R. Gabbrielli, Development of a new steady state zero-dimensional simulation model for woody biomass gasification in a full scale plant, Energy Convers. Manag. 120 (2016) 358–369. doi:

10.1016/j.enconman.2016.05.009.

[21] L. V. Martínez, J. E. Rubiano, M. Figueredo, M. F. Gómez, Experimental study on the performance of gasification of corncobs in a downdraft fixed bed gasifier at various conditions, Renew. Energy 148 (2020) 1216–1226. doi:10.1016/j.renene.2019.10.034.

[22] K. M. Broer, R. C. Brown, The role of char and tar in determining the gas-phase partitioning of nitrogen during biomass gasification, Appl. Energy 158 (2015) 474–483. doi:10.1016/j.apenergy.2015.08.100.

[23] G. Boiger, V. Buff, D. Sharman, M. Boldrini, V. Lienhard, D. Drew, Simulation-based investigation of tar formation in after-treatment systems for biomass gasification, Biomass Conv. Bioref. (2021). doi:10.1007/s13399-020-00915-7.

[24] P. Basu, Biomass Gasification, Pyrolysis and Torrefaction, 3rd Edition, Academic Press, 2018. doi:10.1016/C2016-0-04056-1.

[25] K. Rabea, A. I. Bakry, A. Khalil, M. K. El-Fakharany, M. Kadous, Real-time performance investigation of a downdraft gasifier fueled by cotton stalks in a batch-mode operation, Fuel 300 (2021) 120976. doi:10.1016/j.fuel.2021.120976.

[26] J. D. Martínez, K. Mahkamov, R. V. Andrade, E. E. Silva Lora, Syngas production in downdraft biomass gasifiers and its application using internal combustion engines, Renew. Energy 38 (1) (2012) 1–9. doi:10.1016/j.renene.2011.07.035.

[27] C. Gai, Y. Dong, Experimental study on non-woody biomass gasification in a downdraft gasifier, Int. J. Hydrog. Energy 37 (6) (2012) 4935–4944. doi:10.1016/j.ijhydene.2011.12.031.

[28] A. Saravanakumar, W.-H. Chen, K. D. Arunachalam, Y.-K. Park, H. Chyuan Ong, Pilot-scale study on downdraft gasification of municipal solid waste with mass and energy balance analysis, Fuel 315 (2022) 123287. doi:10.1016/j.fuel.2022.123287.

[29] A. Susastriawan, H. Saptoadi, Purnomo, Small-scale downdraft gasifiers for biomass gasification: A review, Renew. Sust. Energ. Rev. 76 (2017) 989–1003. doi:10.1016/j.rser.2017.03.112.

[30] K. Arun, M. Venkata Ramanan, S. Mohanasutan, Comparative studies and analysis on gasification of coconut shells and corn cobs in a perforated fixed bed downdraft reactor by admitting air through equally spaced conduits, Biomass Conv. Bioref. 12 (2022) 1257–1269. doi:10.1007/s13399-020-00872-1.

[31] M. Awais, M. M. Omar, A. Munir, W. li, M. Ajmal, S. Hussain, S. A. Ahmad, A. Ali, Co-gasification of different biomass feedstock in a pilot-scale (24 kWe) downdraft gasifier: An experimental approach, Energy 238 (2022) 121821. doi:10.1016/j.energy.2021.121821.

[32] L. Devi, K. J. Ptasinski, F. J. Janssen, A review of the primary measures for tar elimination in biomass gasifi-

cation processes, Biomass Bioenergy 24 (2) (2003) 125–140. doi:10.1016/S0961-9534(02)00102-2.

[33] R. Bijesh, P. Arun, C. Muraleedharan, Modified stoichiometric equilibrium model for sewage sludge gasification and its validation based on experiments in a downdraft gasifier, Biomass Conv. Bioref. (2021). doi:10.1007/s13399-021-01916-w.

[34] M. Awais, W. Li, A. Munir, M. M. Omar, M. Ajmal, Experimental investigation of downdraft biomass gasifier fed by sugarcane bagasse and coconut shells, Biomass Conv. Bioref. 11 (2021) 429–444. doi:10.1007/s13399-020-00690-5.

[35] W. Elsner, M. Wysocki, P. Niegodajew, R. Borecki, Experimental and economic study of small-scale CHP installation equipped with downdraft gasifier and internal combustion engine, Appl. Energy 202 (2017) 213–227. doi:10.1016/j.apenergy.2017.05.148.

[36] V. Hansen, D. Müller-Stöver, J. Ahrenfeldt, J. K. Holm, U. B. Henriksen, H. Hauggaard-Nielsen, Gasification biochar as a valuable by-product for carbon sequestration and soil amendment, Biomass Bioenergy 72 (2015) 300–308. doi:10.1016/j.biombioe.2014.10.013.

[37] A. Zabaniotou, D. Rovas, A. Libutti, M. Monteleone, Boosting circular economy and closing the loop in agriculture: Case study of a small-scale pyrolysis-biochar based system integrated in an olive farm in symbiosis with an olive mill, Environ. Dev. 14 (2015) 22–36. doi:10.1016/j.envdev.2014.12.002.

[38] S. Pedrazzi, G. Santunione, A. Minarelli, G. Allesina, Energy and biochar co-production from municipal green waste gasification: A model applied to a landfill in the north of Italy, Energy Convers. Manag. 187 (2019) 274–282. doi:10.1016/j.enconman.2019.03.049.

[39] S. Pedrazzi, G. Santunione, M. Mustone, G. Cannazza, C. Citti, E. Francia, G. Allesina, Techno-economic study of a small scale gasifier applied to an indoor hemp farm: From energy savings to biochar effects on productivity, Energy Convers. Manag. 228 (2021) 113645. doi:10.1016/j.enconman.2020.113645.

[40] S. You, Y. S. Ok, S. S. Chen, D. C. Tsang, E. E. Kwon, J. Lee, C.-H. Wang, A critical review on sustainable biochar system through gasification: Energy and environmental applications, Bioresour. Technol. 246 (2017) 242–253. doi:10.1016/j.biortech.2017.06.177.

[41] N. Hagemann, S. Joseph, H. P. Schmidt, C. I. Kammann, J. Harter, T. Borch, R. B. Young, K. Varga, S. Taherymoosavi, K. W. Elliott, A. McKenna, M. Albu, C. Mayrhofer, M. Obst, P. Conte, A. Dieguez-Alonso, S. Orsetti, E. Subdiaga, S. Behrens, A. Kappler, Organic coating on biochar explains its nutrient retention and stimulation of soil fertility, Nat. Commun. 8 (1) (2017) 1–11. doi:10.1038/s41467-017-01123-0.

[42] G. Allesina, S. Pedrazzi, F. Allegretti, N. Morselli, M. Puglia, G. Santunione, P. Tartarini, Gasification of cotton crop residues for combined power and biochar production in Mozambique, Appl. Therm. Eng. 139

(2018) 387–394. doi:10.1016/j.applthermaleng.2018.04.115.

[43] J. Lehmann, M. C. Rillig, J. Thies, C. A. Masiello, W. C. Hockaday, D. Crowley, Biochar effects on soil biota – a review, Soil Biol. Biochem. 43 (9) (2011) 1812–1836. doi:10.1016/j.soilbio.2011.04.022.

[44] J. Vacheron, G. Desbrosses, M. L. Bouffaud, B. Touraine, Y. Moënne-Loccoz, D. Muller, L. Legendre, F. Wisniewski-Dyé, C. Prigent-Combaret, Plant growth-promoting rhizobacteria and root system functioning, Front. Plant Sci. 4 (2013) 356. doi:10.3389/fpls.2013.00356.

[45] A. Llovet, S. Mattana, J. Chin-Pampillo, G. Gascó, S. Sánchez, C. Mondini, M. J. I. Briones, L. Márquez, J. M. Alcañiz, A. Ribas, X. Domene, Long-term effects of gasification biochar application on soil functions in a Mediterranean agroecosystem: Higher addition rates sequester more carbon but pose a risk to soil faunal communities, Sci. Total Environ. 801 (2021) 149580. doi:10.1016/j.scitotenv.2021.149580.

[46] S. Sri Shalini, K. Palanivelu, A. Ramachandran, V. Raghavan, Biochar from biomass waste as a renewable carbon material for climate change mitigation in reducing greenhouse gas emissions—a review, Biomass Conv. Bioref. (2021). doi:10.1007/s13399-020-00604-5.

[47] R. M. Campbell, N. M. Anderson, D. E. Daugaard, H. T. Naughton, Financial viability of biofuel and biochar production from forest biomass in the face of market price volatility and uncertainty, Appl. Energy 230 (2018) 330–343. doi:10.1016/j.apenergy.2018.08.085.

[48] L. Fryda, R. Visser, Biochar for soil improvement: Evaluation of biochar from gasification and slow pyrolysis, Agriculture 5 (4) (2015) 1076–1115. doi:10.3390/agriculture5041076.

[49] A. Hornung, F. Stenzel, J. Grunwald, Biochar—just a black matter is not enough, Biomass Conv. Bioref. (2021). doi:10.1007/s13399-021-01284-5.

[50] J. Soares, A. C. Oliveira, Experimental assessment of pine wood chips gasification at steady and part-load performance, Biomass Bioenergy 139 (2020) 105625. doi:10.1016/j.biombioe.2020.105625.

[51] L. I. Chaves, M. J. da Silva, S. N. M. de Souza, D. Secco, H. A. Rosa, C. E. C. Nogueira, E. P. Frigo, Small-scale power generation analysis: Downdraft gasifier coupled to engine generator set, Renew. Sust. Energ. Rev. 58 (2016) 491–498. doi:10.1016/j.rser.2015.12.033.

[52] A. K. Sharma, Experimental investigations on a 20 kWe, solid biomass gasification system, Biomass Bioenergy 35 (1) (2011) 421–428. doi:10.1016/j.biombioe.2010.08.060.

[53] Z. Zainal, A. Rifau, G. Quadir, K. Seetharamu, Experimental investigation of a downdraft biomass gasifier, Biomass Bioenergy 23 (4) (2002) 283–289. doi:10.1016/S0961-9534(02)00059-4.

[54] T. Jayah, L. Aye, R. Fuller, D. Stewart, Computer simulation of a downdraft wood gasifier for tea drying, Biomass Bioenergy 25 (4) (2003) 459–469. doi:10.1016/S0961-9534(03)00037-0.

[55] S. Dasappa, D. Subbukrishna, K. Suresh, P. Paul, G. Prabhu, Operational experience on a grid connected 100 kWe biomass gasification power plant in Karnataka, India, Energy Sustain. Dev. 15 (3) (2011) 231–239. doi:10.1016/j.esd.2011.03.004.

[56] R. Yin, R. Liu, J. Wu, X. Wu, C. Sun, C. Wu, Influence of particle size on performance of a pilot-scale fixed-bed gasification system, Bioresour. Technol. 119 (2012) 15–21. doi:10.1016/j.biortech.2012.05.085.

[57] K. X. Kallis, G. A. Pellegrini Susini, J. E. Oakey, A comparison between miscanthus and bioethanol waste pellets and their performance in a downdraft gasifier, Appl. Energy 101 (2013) 333–340. doi:10.1016/j.apenergy.2012.01.037.

[58] U. Lee, E. Balu, J. Chung, An experimental evaluation of an integrated biomass gasification and power generation system for distributed power applications, Appl. Energy 101 (2013) 699–708. doi:10.1016/j.apenergy.2012.07.036.

[59] N. Nwokolo, S. Mamphweli, E. Meyer, S. Tangwe, Electrical performance evaluation of Johansson biomass gasifier system coupled to a 150 kVA generator, Renew. Energy 71 (2014) 695–700. doi:10.1016/j.renene.2014.06.018.

[60] S. Sarker, H. K. Nielsen, Assessing the gasification potential of five woodchips species by employing a lab-scale fixed-bed downdraft reactor, Energy Convers. Manag. 103 (2015) 801–813. doi:10.1016/j.enconman.2015.07.022.

[61] M. Simone, F. Barontini, C. Nicolella, L. Tognotti, Gasification of pelletized biomass in a pilot scale downdraft gasifier, Bioresour. Technol. 116 (2012) 403–412. doi:10.1016/j.biortech.2012.03.119.

[62] P. R. Bhoi, R. L. Huhnke, A. Kumar, S. Thapa, N. Indrawan, Scale-up of a downdraft gasifier system for commercial scale mobile power generation, Renew. Energy 118 (2018) 25–33. doi:10.1016/j.renene.2017.11.002.

[63] E. Biagini, F. Barontini, L. Tognotti, Gasification of agricultural residues in a demonstrative plant: Vine pruning and rice husks, Bioresour. Technol. 194 (2015) 36–42. doi:10.1016/j.biortech.2015.07.016.

[64] C. Li, Y. Shen, J. Wu, Y. Dai, C.-H. Wang, Experimental and modeling investigation of an integrated biomass gasifier–engine–generator system for power generation and waste heat recovery, Energy Convers. Manag. 199 (2019) 112023. doi:10.1016/j.enconman.2019.112023.

[65] M. R. Kabli, A. M. Ali, M. Inayat, A. A. Zahrani, K. Shahzad, M. Shahbaz, S. A. Sulaiman, H_2-rich syngas production from air gasification of date palm waste: an experimental and modeling investigation, Biomass Conv. Bioref. (2022). doi:10.1007/s13399-022-02375-7.

[66] M. La Villetta, M. Costa, D. Cirillo, N. Massarotti, L. Vanoli, Performance analysis of a biomass powered

micro-cogeneration system based on gasification and syngas conversion in a reciprocating engine, Energy Convers. Manag. 175 (2018) 33–48. doi:10.1016/j.enconman.2018.08.017.

[67] C. Rodríguez Coronado, J. Tiyoko Yoshioka, J. Luz Silveira, Electricity, hot water and cold water production from biomass. energetic and economical analysis of the compact system of cogeneration run with woodgas from a small downdraft gasifier, Renew. Energy 36 (6) (2011) 1861–1868. doi:10.1016/j.renene.2010.11.021.

[68] N. Proenza Pérez, E. Blanco Machín, D. Travieso Pedroso, J. J. Roberts, J. Santana Antunes, J. Luz Silveira, Biomass gasification for combined heat and power generation in the Cuban context: Energetic and economic analysis, Appl. Therm. Eng. 90 (2015) 1–12. doi:10.1016/j.applthermaleng.2015.06.095.

[69] F. Patuzzi, D. Basso, S. Vakalis, D. Antolini, S. Piazzi, V. Benedetti, E. Cordioli, M. Baratieri, State-of-the-art of small-scale biomass gasification systems: An extensive and unique monitoring review, Energy 223 (2021) 120039. doi:10.1016/j.energy.2021.120039.

[70] P. Kumar, P. Subbarao, L. Kala, V. Vijay, Experimental assessment of producer gas generation using agricultural and forestry residues in a fixed bed downdraft gasifier, Chem. Eng. J. Adv. 13 (2023) 100431. doi:10.1016/j.ceja.2022.100431.

[71] S. J. Yoon, Y.-I. Son, Y.-K. Kim, J.-G. Lee, Gasification and power generation characteristics of rice husk and rice husk pellet using a downdraft fixed-bed gasifier, Renew. Energy 42 (2012) 163–167. doi:10.1016/j.renene.2011.08.028.

[72] R. D. Gómez, M. Palacio, J. F. Arango, A. E. Ávila, J. M. Mendoza, Evaluation of the energy generation potential by an experimental characterization of residual biomass blends from Córdoba, Colombia in a downdraft gasifier, Waste Manage. 120 (2021) 522–529. doi:10.1016/j.wasman.2020.10.014.

[73] W. B. Wincy, M. Edwin, S. J. Sekhar, Energy and exergy evaluation of rice processing mills working with biomass gasifier in parboiling process, Fuel 259 (2020) 116255. doi:10.1016/j.fuel.2019.116255.

[74] W. B. Wincy, M. Edwin, S. J. Sekhar, Exergetic evaluation of a biomass gasifier operated reversible flatbed dryer for paddy drying in parboiling process, Biomass Conv. Bioref. (2021). doi:10.1007/s13399-021-01322-2.

[75] W. B. Wincy, M. Edwin, Experimental energy, exergy, and exergoeconomic (3E) analysis of biomass gasifier operated paddy dryer in parboiling industry, Biomass Conv. Bioref. (2022). doi:10.1007/s13399-021-02156-8.

[76] V. C. Jeya Singh, S. J. Sekhar, Performance studies on a downdraft biomass gasifier with blends of coconut shell and rubber seed shell as feedstock, Appl. Therm. Eng. 97 (2016) 22–27. doi:10.1016/j.applthermaleng.

2015.09.099.

[77] M. Dogru, C. Howarth, G. Akay, B. Keskinler, A. Malik, Gasification of hazelnut shells in a downdraft gasifier, Energy 27 (5) (2002) 415–427. doi:10.1016/S0360-5442(01)00094-9.

[78] S. Mazhkoo, H. Dadfar, M. HajiHashemi, O. Pourali, A comprehensive experimental and modeling investigation of walnut shell gasification process in a pilot-scale downdraft gasifier integrated with an internal combustion engine, Energy Convers. Manag. 231 (2021) 113836. doi:10.1016/j.enconman.2021.113836.

[79] E. Biagini, F. Barontini, L. Tognotti, Gasification of agricultural residues in a demonstrative plant: Corn cobs, Bioresour. Technol. 173 (2014) 110–116. doi:10.1016/j.biortech.2014.09.086.

[80] P. García-Ibáñez, A. Cabanillas, J. Sánchez, Gasification of leached orujillo (olive oil waste) in a pilot plant circulating fluidised bed reactor. Preliminary results, Biomass Bioenergy 27 (2) (2004) 183–194. doi:10.1016/j.biombioe.2003.11.007.

[81] M. Dogru, A. Erdem, Autothermal fixed bed updraft gasification of olive pomace biomass and renewable energy generation via Organic Rankine Cycle turbine : Green energy generation from waste biomass in the Mediterranean region, Johnson Matthey Technol. Rev. 64 (2) (2020) 119–134. doi:10.1595/205651320X15746781209529.

[82] V. R. Patel, D. S. Upadhyay, R. N. Patel, Gasification of lignite in a fixed bed reactor: Influence of particle size on performance of downdraft gasifier, Energy 78 (2014) 323–332. doi:10.1016/j.energy.2014.10.017.

[83] M. Baratieri, P. Baggio, B. Bosio, M. Grigiante, G. Longo, The use of biomass syngas in IC engines and CCGT plants: A comparative analysis, Appl. Therm. Eng. 29 (16) (2009) 3309–3318. doi:10.1016/j.applthermaleng.2009.05.003.

[84] M. L. Valderrama Ríos, A. Martínez González, E. E. Silva Lora, O. A. Almazán del Olmo, Reduction of tar generated during biomass gasification: A review, Biomass Bioenergy 108 (2018) 345–370. doi:10.1016/j.biombioe.2017.12.002.

[85] M. Costa, M. La Villetta, N. Massarotti, D. Piazzullo, V. Rocco, Numerical analysis of a compression ignition engine powered in the dual-fuel mode with syngas and biodiesel, Energy 137 (2017) 969–979. doi:10.1016/j.energy.2017.02.160.

[86] A. M. Salem, I. N. Zaini, M. C. Paul, W. Yang, The evolution and formation of tar species in a downdraft gasifier: Numerical modelling and experimental validation, Biomass Bioenergy 130 (2019) 105377. doi:10.1016/j.biombioe.2019.105377.

[87] P. Oosthuizen, W. Carscallen, Introduction to Compressible Fluid Flow, 2nd Edition, CRC Press, 2013. doi:10.1201/b15414.

[88] F. Patuzzi, D. Prando, S. Vakalis, A. M. Rizzo, D. Chiaramonti, W. Tirler, T. Mimmo, A. Gasparella, M. Baratieri, Small-scale biomass gasification CHP systems: Comparative performance assessment and monitoring experiences in South Tyrol (Italy), Energy 112 (2016) 285–293. doi:10.1016/j.energy.2016.06.077.

[89] S. Vecten, M. Wilkinson, N. Bimbo, R. Dawson, B. M. Herbert, Hydrogen-rich syngas production from biomass in a steam microwave-induced plasma gasification reactor, Bioresour. Technol. 337 (2021) 125324. doi:10.1016/j.biortech.2021.125324.

[90] R. Kramreiter, M. Url, J. Kotik, H. Hofbauer, Experimental investigation of a 125 kW twin-fire fixed bed gasification pilot plant and comparison to the results of a 2 MW combined heat and power plant (CHP), Fuel Process. Technol. 89 (1) (2008) 90–102. doi:10.1016/j.fuproc.2007.08.001.

[91] S. McAllister, J.-Y. Chen, A. C. Fernández-Pello, Fundamentals of Combustion Processes, Springer, 2011. doi:10.1007/978-1-4419-7943-8.

[92] N. Fonseca González, J. Casanova Kindelán, J. M. López Martínez, Methodology for instantaneous average exhaust gas mass flow rate measurement, Flow Meas. Instrum. 49 (2016) 52–62. doi:10.1016/j.flowmeasinst.2016.04.007.

[93] International Bureau of Weights and Measures, Guide to the Expression of Uncertainty in Measurement, https://www.bipm.org/documents/20126/2071204/JCGM_100_2008_E.pdf/cb0ef43f-baa5-11cf-3f85-4dcd86f77bd6, Accessed: 2022-06-18 (2008).

[94] R. A. M. Boloy, J. L. Silveira, C. E. Tuna, C. R. Coronado, J. S. Antunes, Ecological impacts from syngas burning in internal combustion engine: Technical and economic aspects, Renew. Sust. Energ. Rev. 15 (9) (2011) 5194–5201. doi:10.1016/j.rser.2011.04.009.

[95] W. van de Kamp, P. de Wild, H. Knoef, J. Neeft, J. Kiel, Tar measurement in biomass gasification, standardisation and supporting R&D, Available at: https://publications.ecn.nl/E/2006/ECN-C--06-046, Accessed: 2023-03-02.

[96] M. Wegener, A. Malmquist, A. Isalgué, A. Martin, Biomass-fired combined cooling, heating and power for small scale applications – A review, Renew. Sust. Energ. Rev. 96 (2018) 392–410. doi:10.1016/j.rser.2018.07.044.

[97] S. Tsiakmakis, D. Mertzis, A. Dimaratos, Z. Toumasatos, Z. Samaras, Experimental study of combustion in a spark ignition engine operating with producer gas from various biomass feedstocks, Fuel 122 (2014) 126–139. doi:10.1016/j.fuel.2014.01.013.

[98] Commission Regulation (EU) 2016/631 of 14 April 2016 establishing a network code on requirements

for grid connection of generators, https://eur-lex.europa.eu/legal-content/EN/TXT/?uri=CELEX:32016R0631 (2016).

[99] P. Breeze, Piston Engine Combined Heat and Power Systems, in: P. Breeze (Ed.), Combined Heat and Power, Academic Press, 2018, pp. 33–40. doi:10.1016/B978-0-12-812908-1.00004-3.

[100] C. Li, J. Wu, Y. Shen, X. Kan, Y. Dai, C.-H. Wang, Evaluation of a combined cooling, heating, and power system based on biomass gasification in different climate zones in the U.S., Energy 144 (2018) 326–340. doi:10.1016/j.energy.2017.12.021.